Qiao et al. *Zool. Res.* 2025, 46(5): 1059−1078
https://doi.org/10.24272/j.issn.2095-8137.2025.057
https://cstr.cn/32248.14.zr.2025.057

ZR | Zoological Research

Article Open Access

Taxonomy, phylogeny, and biogeography of the Oriental subfamily Perittopinae China & Usinger, 1949 (Hemiptera: Heteroptera: Veliidae)

Mu Qiao[1,#], Ze-Zhong Jin[1,#], Herbert Zettel[2,*], Katharina Ehrengruber[2], Chen Liu[1], Zi-He Li[1], Zhao-Qi Leng[1], Si-Ying Fu[1], Wen-Jun Bu[1,*], Zhen Ye[1,*]

[1] *Institute of Entomology*, *College of Life Sciences*, *Nankai University*, *Tianjin* 300071, *China*
[2] *2nd Zoological Department*, *Natural History Museum Vienna*, *Vienna* 1010, *Austria*

ABSTRACT

The collision of the Indian and Eurasian plates during the Eocene represents a major tectonic shift that significantly altered biotic dynamics and promoted species diversification across the Oriental region. To explain the diversification of taxa from the Indian subcontinent into Southeast Asia, two principal hypotheses have been proposed: the “Biotic-ferry” and “Step-stone” models. The subfamily Perittopinae, a lineage of semi-aquatic bugs comprising a single genus and 20 extant species, provides an ideal system for testing these hypotheses due to its disjunct distribution spanning the Indian subcontinent and Southeast Asia. This study conducted a comprehensive taxonomic analysis of the entire subfamily, incorporating newly defined morphological characters and multilocus phylogenetic analyses to reconstruct evolutionary relationships and historical biogeography. Morphological and phylogenetic evidence confirmed the monophyly of Perittopinae and supported the establishment of three new genera—*Indoperittopus* **gen. nov.**, *Pachyperittopus* **gen. nov.**, and *Falciperittopus* **gen. nov.**—in addition to four new species and four new combinations. Biogeographic reconstructions indicated a southern Indian origin, with initial diversification potentially occurring during the mid-Paleocene, coinciding with the major phases of the India-Eurasia collision. Subsequent range expansion over marine barriers facilitated colonization of the northern Sunda Shelf, consistent with the “Step-stone” dispersal mechanism. Later northward expansion from the southern Sunda Shelf during the early Miocene triggered further diversification of the genus *Perittopus* within the Indo-China Peninsula. These findings advance understanding of Perittopinae systematics, phylogeny, and historical biogeography, identifying the northward drift of the Indian plate and its eventual collision with Eurasia as catalysts of diversification within this semi-aquatic lineage.

Keywords: Diversification; Historical biogeography; India-Eurasia collision; Perittopinae; Phylogeny; Taxonomy

INTRODUCTION

The Indian subcontinent, originally part of Gondwana, collided with the Eurasian landmass derived from Laurasia during the Eocene (Chatterjee et al., 2013; Torsvik & Cocks, 2013), marking a tectonic event of profound geobiological consequence. Paleogeographic reconstructions indicate initial contact around 55±5 million years ago (Ma), with full convergence occurring by approximately 40±5 Ma (Wu et al., 2023). Although the precise chronology and trajectory of this tectonic convergence remain subjects of ongoing debate (Aitchison et al., 2007; Ali & Aitchison, 2008; Beck et al., 1995; van Hinsbergen et al., 2012; Yin & Harrison, 2000), mounting evidence implicates this collision as a major driver of intercontinental biotic exchange. This includes transcontinental dispersal of Gondwanan lineages into Southeast Asia, lending support to the “Out of India” hypothesis (Grismer et al., 2016; Klaus et al., 2016; Loria & Prendini, 2020). The biogeographic legacy of this event is widely considered as a primary contributor to the exceptional species richness of Southeast Asia, a region recognized as a global biodiversity hotspot (Datta-Roy & Karanth, 2009; Gower et al., 2002).

Prior to this continental convergence, faunal assemblages on the Indian subcontinent, isolated following its separation from Gondwana, exhibited pronounced endemism and

This is an open-access article distributed under the terms of the Creative Commons Attribution Non-Commercial License (http://creativecommons.org/licenses/by-nc/4.0/), which permits unrestricted non-commercial use, distribution, and reproduction in any medium, provided the original work is properly cited.

Copyright ©2025 Editorial Office of Zoological Research, Kunming Institute of Zoology, Chinese Academy of Sciences

Received: 28 April 2025; Accepted: 01 September 2025; Online: 02 September 2025

Foundation items: This work was supported by the Natural Science Foundation of Tianjin, China (24JCYBJC01910) and National Natural Science Foundation of China (32322012, 32470467)

[#]Authors contributed equally to this work

*Corresponding authors, E-mail: herbert.zettel@nhm-wien.ac.at; wenjunbu@nankai.edu.cn; yezhen1987331@nankai.edu.cn

regional distinctiveness (Keast, 1971). Thus, the Indian subcontinent served as a "biotic ferry", facilitating species exchange with the Eurasian continent after tectonic collision enabled overland dispersal (Foley et al., 2021; Li et al., 2013; Palmieri et al., 2023; Yamahira et al., 2021). However, emerging evidence challenges the assumption of complete isolation during the northward migration of the Indian plate. The "Step-stone" biogeographic model proposed by Yuan et al. (2019) posits that species may have dispersed across marine barriers via transient island arcs or land bridge formations. Following the collision, dispersal routes of many lineages extended eastward toward the Sunda Shelf rather than northward, likely constrained by geographical barriers and climatic factors (Gorin et al., 2020; Li et al., 2020; Morley, 2018). This pattern may be linked to a preceding India-arc collision, which potentially created temporary dispersal corridors into western Sundaland well before the establishment of continuous land connections between India and continental Asia (Hall, 2013).

In parallel, tectonism across Southeast Asia exerted substantial influence on regional diversification dynamics. Notably, uplift of the Qinghai-Xizang Plateau, triggered by continental collision, significantly reshaped monsoonal systems and climatic gradients (Chatterjee et al., 2013; Favre et al., 2015; Zhang et al., 2024). From the Paleocene to mid-Oligocene, Sundaland existed as a prominent peninsula along the southern margin of Eurasia. Approximately 20 Ma, tectonic movements initiated the gradual isolation of islands, as exemplified by the geodynamic evolution of Borneo (Hall, 2013; Lohman et al., 2011). Concurrent sea-level fluctuations further altered island connectivity, profoundly influencing species formation and diversification across archipelagic systems (Klaus et al., 2013; Sholihah et al., 2021a, 2021b; Sitam et al., 2023). Subsequent to the Miocene, uplift of the Hengduan Mountains established extensive geographic isolation in this biodiversity hotspot, further intensifying speciation processes (He et al., 2021; Kou et al., 2023; Zhao et al., 2021).

Perittopinae China & Usinger, 1949 represents a small morphologically distinct subfamily within the family Veliidae (riffle bugs), comprising small-bodied, often vividly colored semi-aquatic insects. Most species exhibit bright red or orange dorsal coloration, with some bearing conspicuous black markings or patches. Hitherto, the subfamily was considered monogeneric, including only the genus *Perittopus* Fieber, 1860, encompassing 20 described species distributed throughout the Oriental Realm, including Sri Lanka, India, Southeast Asian mainland (e.g, southwestern China and Indo-China Peninsula), and the western Sunda Islands (e.g., Sumatra, Java, Bali, and Borneo) (Figure 1). Eastern range limits correspond with the biogeographic boundary of Wallace's Line, as modified by Huxley (1868). Taxonomic revision of *Perittopus* was first undertaken by Lundblad (1933) in a comprehensive treatment that addressed all but one species (*Perittopus maculatus* Paiva, 1919; see Zenz & Zettel, 2021). Since then, species discoveries have expanded the genus, particularly in West Malesia (Zettel, 2001a), Southeast Asia (Ye et al., 2013, 2020; Zettel, 2001a, 2011), and Sri Lanka (Zettel, 2001b) (Supplementary Table S1). Historical taxonomic developments and persisting classification challenges are summarized in the Supplementary Text. The phylogenetic position of the Perittopinae was first discussed by Andersen (1982). Perittopinae has long been recognized as an independent clade within Veliidae, distinct from both Rhagoveliinae and Veliinae, with no known synapomorphic characters supporting a close relationship among these subfamilies (Andersen, 2000; Andersen & Weir, 2004; Damgaard, 2008, 2012; Polhemus, 1997). While higher-level phylogenetic placement of Perittopinae has received attention, interspecific relationships within the subfamily and its historical biogeography remain unresolved.

This study presents the first integrative phylogenetic and taxonomic revision of the entire subfamily, including the establishment of new genera, new species, and new combinations. A comprehensive molecular dataset was assembled encompassing all 13 protein-coding genes (PCGs), 12S and 16S mitochondrial DNA (rDNA), nuclear 18S and 28S rDNA, and a matrix of 68 newly redefined morphological characters specific to Perittopinae. These data were used to construct a robust phylogenetic framework and infer divergence times through fossil-calibrated molecular dating. Diversification rate analyses and ancestral ranges reconstruction were conducted to evaluate alternative historical biogeographic models—specifically, the "Biotic ferry" and "Step-stone" hypotheses—providing new insight into the evolutionary dynamics and geographic expansion of this lineage.

MATERIALS AND METHODS

Taxon sampling

A total of 462 specimens, deposited across six institutional collections (Supplementary Table S2), were included in taxonomic, morphological, and phylogenetic analyses. The sampling encompassed 23 recognized species, including newly described taxa, with the exception of the controversial species *Perittopus rufus* (Supplementary Tables S1, S3). Ten additional species representing four gerromorphan families (Mesoveliidae, Hydrometridae, Gerridae, and Veliidae) were selected as outgroups to capture broad phylogenetic diversity within the infraorder and to anchor fossil-calibrated nodes for divergence time estimation (Supplementary Tables S3, S4).

Taxonomic and morphological phylogenetic analyses

All available Perittopinae specimens were analyzed (Supplementary Table S1), including holotypes of 16 species (Supplementary Figure S1), among them the newly described taxa. Material housed at the Institute of Entomology, College of Life Sciences, Nankai University, Tianjin, China (NKUM) (Supplementary Table S2) was analyzed using a ZEISS SteREO Discovery V8 optical microscope (Germany). Dorsal views and structural details were captured using a Canon EOS600d stereomicroscope (China) equipped with a computer-controlled SPOTRT digital camera, with image capture and processing conducted using Helicon Remote v.3.9.12 W and Helicon Focus v.7.7.5. Dissected genitalia were photographed using an Olympus BX53 microscope (Japan) equipped with a computer-controlled Canon OLYMPUS DP72 digital camera (Japan) and cellSens Standard v.1.6. New species and combinations deposited in the Natural History Museum, London, United Kingdom (BMNH), Hungarian Museum of Natural Sciences, Budapest, Hungary (MTMB), Naturhistorisches Museum Vienna, Austria (NHMW), Naturhistoriska Riksmuseet, Stockholm, Sweden (NHRS), and Zoologisches Museum und Universität Kopenhagen, Denmark (ZMUC) (Supplementary Table S2)

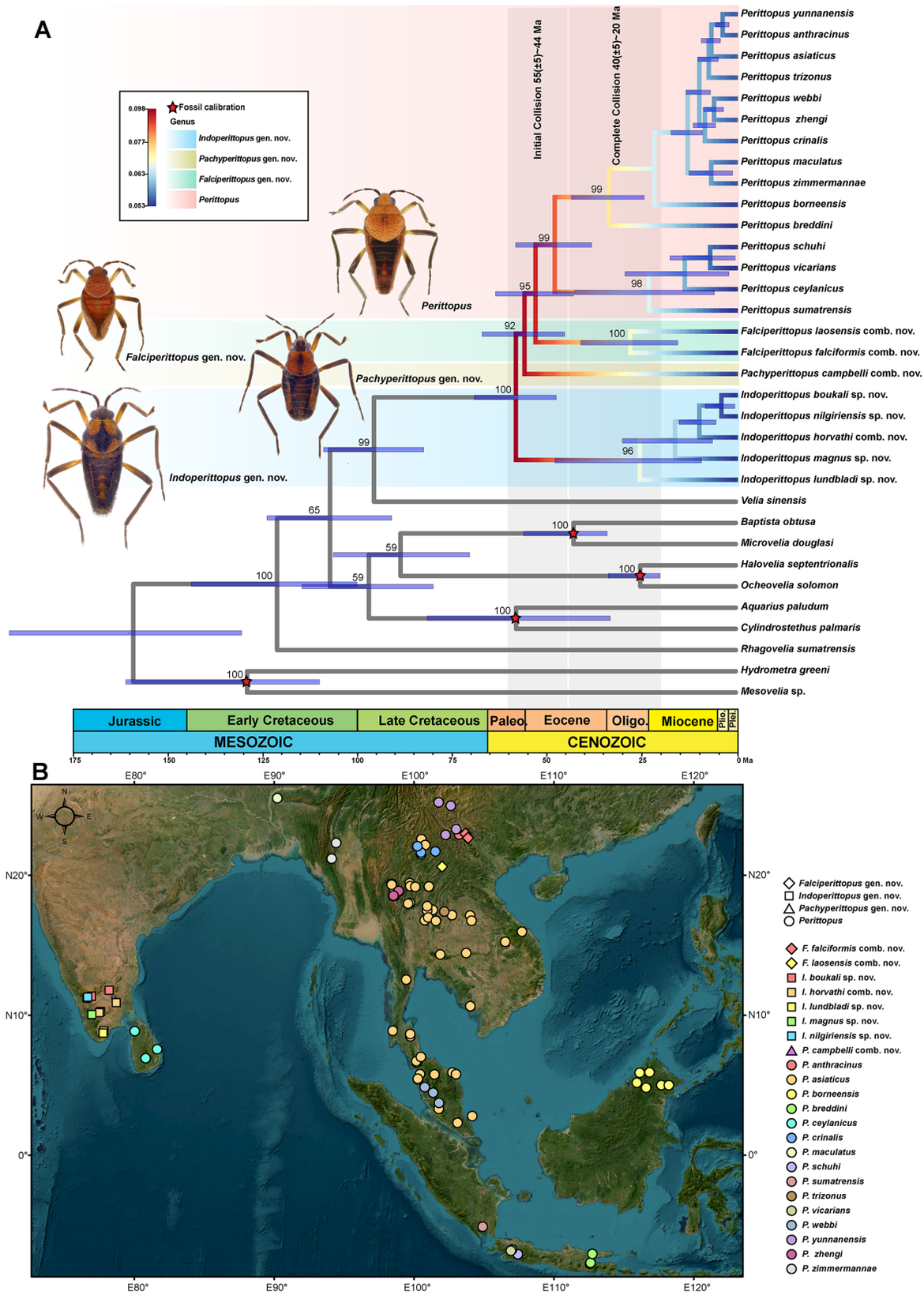

Figure 1 Phylogenetic reconstructions, divergence time estimations, and diversification rate analyses of the subfamily Perittopinae

A: Phylogenetic tree was constructed based on 33 samples from the PCG_12S16S_18S28S_MORPH matrix using maximum-likelihood (ML) analysis. The 95% highest posterior density (HPD) intervals, indicated by blue bars, were estimated using BEAST2. Bootstrap values were annotated. Diversification rate analysis of the ingroup was conducted using BAMM. Red stars represent fossil calibration points and colors of ingroup tree reflect speciation rates. Specimens on the right, arranged from top to bottom, represent *Perittopus*, *Falciperittopus* gen. nov., *Pachyperittopus* gen. nov., and *Indoperittopus* gen. nov. B: Schematic map showing distribution of Perittopinae based on all known collection records.

were examined using a Leica Wild M10 binocular microscope (Germany). Genital segments were examined under a Leica MZ12 compound microscope (Germany). Dorsal views and structural details were captured with a Leica DFC450 camera mounted on a Leica Z16APO carrier and processed using Leica Application Suite v.3.8 (Germany). Morphometric data were collected using a Nikon SMZ1500 binocular microscope (Japan), and all illustrations were compiled and finalized in Adobe Photoshop CC 2018.

Fifty-nine binary and multistate morphological characters were selected across 23 Perittopinae species for phylogenetic analysis (Supplementary Tables S9, S10). *Velia sinensis* was designated as the outgroup. For taxa unavailable for direct observation, selected morphological characters were derived from published literature (Supplementary Table S1). Character matrix construction was performed using WinClada v.1.00.08 (Nixon, 2002). Maximum-parsimony (MP) analysis was carried out via traditional heuristic search under default parameters in TNT v.1.5 (Goloboff & Catalano, 2016), with all characters treated as non-additive. Consensus trees were generated using the 50% majority rule method. Clade robustness was evaluated with jackknife resampling and standard bootstrap reweighting values (1 000 replicates). Maximum-likelihood (ML) analysis was performed using IQ-TREE2 (Minh et al., 2020).

Molecular procedures, sequencing, and alignment

Complete sequences of all 13 mitochondrial PCGs, mitochondrial 12S and 16S rDNA, and nuclear 18S and 28S rDNA were newly generated for 15 Perittopinae species (Supplementary Table S3). Total genomic DNA was extracted from alcohol-preserved specimens stored at −20℃ using the DNeasy Tissue Kit (Kangwei, China). Libraries were constructed with a 250 bp insert size and sequenced using a 150 bp paired-end strategy on the Illumina HiSeq 4000 platform at Novogene (Tianjin, China), yielding approximately 2 Gb of clean reads per sample. Mitochondrial genome assemblies were performed using MitoZ (Meng et al., 2019), MITObim (Hahn et al., 2013), Geneious Prime v.2022.2 (https://www.geneious.com), and IDBA-UD (Peng et al., 2012). Nuclear 18S and 28S rDNA sequences were retrieved from assembled data using BLAST+ (Camacho et al., 2009). The 13 mitochondrial PCGs were identified with ORF Finder (https://www.ncbi.nlm.nih.gov/orffinder/) under the invertebrate mitochondrial genetic code, validated against published hemipteran mitochondrial sequences using BLAST (http://blast.ncbi.nlm.nih.gov/Blast.cgi). Annotations of mitochondrial 12S and 16S rDNA were based on conserved gene arrangement and verified manually using reference datasets. Each PCG was aligned in codon mode using MAFFT v.7.313 (Katoh & Standley, 2013), with terminal stop codons excluded. Alignments of nuclear 18S and 28S rDNA were conducted using MAFFT v.7.313 in normal mode. Regions of questionable homology were removed using Gblocks v.0.91 (Talavera & Castresana, 2007), implemented within PhyloSuite v.1.2.2 (Zhang et al., 2020).

Phylogenetic analyses of combined datasets

Molecular and morphological data were concatenated into three combined matrices: PCG_12S16S_18S28S_MORPH (comprising all three codon positions of the 13 mitochondrial PCGs, mitochondrial 12S rDNA, mitochondrial 16S rDNA, nuclear 18S rDNA, nuclear 28S rDNA, and morphological characteristics), PCG_12S16S (comprising all three codon positions of the 13 mitochondrial PCGs, mitochondrial 12S rDNA, and mitochondrial 16S rDNA), and 18S28S (comprising nuclear 18S and 28S rDNA). The first matrix served as the primary analytical framework, while the latter two acted as supplementary datasets to accommodate taxa lacking complete molecular data. The concatenated nucleotide dataset contained 25 sequences representing 25 species, with missing data comprising less than 1.2% of the matrix. For each PCG, 12S rDNA, 16S rDNA, 18S rDNA, 28S rDNA, and morphological partition within the nucleotide matrix, ModelFinder (Kalyaanamoorthy et al., 2017) was used to infer the best partitioning strategy and substitution model under Bayesian information criterion (BIC) (Supplementary Table S5). The morphological matrix consisted of 59 characters scored across 24 species, all newly generated in the present study (Supplementary Tables S9, S10). Phylogenetic inference was conducted using IQ-TREE2 (Minh et al., 2020) for ML and TNT v.1.5 (Goloboff & Catalano, 2016) for MP. ML analyses incorporated the ultrafast bootstrap approach with 5 000 replicates to assess node support, while all other parameters followed default settings. MP analyses were performed using a traditional heuristic search under default settings. Consensus trees were generated using the 50% majority rule consensus. Clade robustness was evaluated with jackknife resampling and standard bootstrap reweighting values (1 000 replicates).

Divergence time estimation

Divergence times were estimated using BEAST v.2.6.6 (Bouckaert et al., 2014) under a birth-death tree prior and a relaxed clock model with a lognormal distribution to accommodate lineage-specific variation (Drummond et al., 2006). The PCG_12S16S_18S28S_MORPH dataset was partitioned into nucleotide and morphological matrices. The GTR substitution model, identified via ModelFinder embedded in PhyloSuite, was applied to all nucleotide partitions. The MK model, implemented through the morph-models package in BEAST, was selected for the morphological partition. Despite the absence of crown-group Perittopinae fossils, divergence time estimation was anchored using seven rigorously constrained fossil calibrations from three gerromorphan outgroup families (Supplementary Table S4), with all fossil occurrences verified through the Paleobiology Database (https://www.paleobiodb.org/). The calibration scheme followed the framework established by Ye et al. (2024) for the subfamily Haloveliinae in Veliidae, applying identical fossil anchors to calibrate their respective adjacent ancestral nodes (Supplementary Table S4). Soft bounds were used on all calibrations, and exponential priors were favored over lognormal distributions, as they require fewer parameters and are more appropriate when fossil records are sparse or uneven (Ho & Phillips, 2009). Default priors were retained for all other parameters in BEAUti. The analysis was run for 3×10^9 generations and sampled every 1 000 generations. Convergence was monitored using Tracer v.1.7 ((Rambaut et al., 2018), and all effective sample size (ESS) values exceeded the threshold of 200. TreeAnnotator (Bouckaert et al., 2014) was used to generate a maximum clade credibility (MCC) chronogram from the post-burn-in tree set (first 25% discarded as burn-in), summarizing mean divergence time estimates with 95% highest posterior density (HPD) intervals.

Diversification rate analysis

Species diversification dynamics were reconstructed using

BAMM v.2.5.0 to estimate temporal and lineage-specific variation in speciation (λ) and extinction (μ) rates across the Perittopinae phylogeny (Rabosky et al., 2013). Prior distributions for λ and μ were computed using the R package BAMMtools (Rabosky et al., 2014), with parameters lambdaInitPrior=4.75475679984377, lambdaShiftPrior= 0.019828050082928, and muInitPrior=4.75475679984377. The analysis was run for 5 million generations and sampled every 1 000 generations. Convergence was assessed by log-likelihood traces and ESSs (>200) of the log-likelihood. Heterogeneity in diversification dynamics among branches was evaluated using two approaches in BAMMtools: (i) mean phylorate plot depicting distinct branch-specific speciation rates via color gradients, and (ii) rate-through-time analysis tracking net diversification, speciation, and extinction rates across the tree. To independently validate patterns of diversification rate heterogeneity, the ClaDS2 model (Maliet et al., 2019) was implemented using the "*fit_ClaDS*" function in the "RPANDA" R package. This approach employed three chains of blocked differential evolution (DE) Markov chain Monte Carlo (DE-MCMC) sampling over 10 000 generations. Posterior estimates of branch-specific speciation rates were extracted using the "*getMAPS_ClaDS*" function to obtain the maximum *a posteriori* values for each parameter.

Ancestral range estimation

Ancestral geographic distributions were reconstructed using the ingroup subtree of the BEAST-derived MCC phylogeny. Outgroup taxa were manually pruned by editing the Newick-formatting tree prior. Biogeographic inference was conducted in BioGeoBEARS v.1.1.3 (https://github.com/nmatzke/BioGeoBEARS), which incorporates a parameter describing founder-event speciation (+j) likely to be important in oceanic settings (Matzke, 2014) and allows the comparison of different models in a statistical framework. Species distribution data were compiled from examined material and literature records (Lundblad, 1933; Ye at al., 2013, 2020; Zenz & Zettel, 2021; Zettel, 2001a, 2001b). Terminal taxa were assigned to three biogeographic areas based on palaeogeographical reconstructions and species-specific range data (Gorin et al., 2020; Li et al., 2020; Morley, 2018; Yuan et al., 2019): (A) South India and Sri Lanka; (B) Indo-China Peninsula; and (C) Malesia, including West Malaysia, Sumatra, Java, and Borneo (Supplementary Table S6). Two temporally explicit dispersal scenarios were considered to represent the "Step-stone" and "Biotic-ferry" models (Yuan et al., 2019), corresponding to the time intervals 0–55 Ma and 55–60 Ma. Dispersal rate matrices were scales to reflect geological history, the presence and dissolution of land bridges, and island arc formation, ranging from 0.01 for well-separated areas to 1.00 for contiguous landmasses (Supplementary Table S7). Model comparisons were conducted using uncorrected Akaike Information Criterion (AIC) across three fundamental models: Dispersal-Extinction-Cladogenesis model (DEC; Ree & Smith, 2008), Dispersal-Vicariance Analysis-like model (DIVALIKE; Ronquist, 1997), and BayArea-like model (BAYAREALIKE; Landis et al., 2013). To address concerns regarding model comparability (Ree & Sanmartín, 2018), a parallel comparative framework was implemented for their respective +J variants (DEC+J, DIVALIKE+J, and BAYAREALIKE+J). Within each group, models were evaluated using AIC, with ΔAIC>2 indicative of substantial support. Ancestral state reconstruction was constrained to a maximum of two regions per node. Likelihood-ratio tests and AIC were used to identify the best-fitting model (Supplementary Table S8).

RESULTS

Morphological analyses

Morphological analyses resolved three distinct and monophyletic lineages corresponding to the newly proposed genera: *Indoperittopus* **gen. nov.**, *Pachyperittopus* **gen. nov.**, and *Falciperittopus* **gen. nov.** (Figures 3–5). Combined phylogenetic reconstruction incorporating molecular and morphological data further supported these generic boundaries, with ML bootstrap values ranging from 92 to 100 (Figure 1A). *Indoperittopus* **gen. nov.** comprises five species, including four newly described taxa: *Indoperittopus boukali* **sp. nov.**, *Indoperittopus nilgiriensis* **sp. nov.**, *Indoperittopus magnus* **sp. nov.** and *Indoperittopus lundbladi* **sp. nov.** The fifth species, *Indoperittopus horvathi* **comb. nov.**, was reassigned from *Perittopus* to *Indoperittopus* based on shared morphological characteristics (see taxonomic section). *Falciperittopus falciformis* **comb. nov.** and *Falciperittopus laosensis* **comb. nov.**, also previously placed in *Perittopus*, were transferred to the newly established genus *Falciperittopus* **gen. nov.** due to distinct morphological synapomorphies. *Pachyperittopus* **gen. nov.**, represented by *Pachyperittopus campbelli* **comb. nov.** (formerly *Perittopus campbelli*), was distinguished by a unique suite of structural features justifying its recognition as a separate genus. Phylogenetic analysis based solely on morphological characters (Supplementary Figure S2) further substantiated the establishment of the three new genera. The resulting topology recovered *Perittopus* and *Falciperittopus* **gen. nov.** as sister lineages, with *Indoperittopus* **gen. nov.** positioned at the base of the subfamily. The relationships among the four genera are represented as (*Indoperittopus* **gen. nov.** + (*Pachyperittopus* **gen. nov.** + (*Falciperittopus* **gen. nov.** + *Perittopus*))) (Figure 1A).

Combined dataset phylogenetic analyses

The combined PCG_12S16S_18S28S_MORPH dataset included 19 039 nucleotide positions and 59 discrete morphological characters. ML analysis of the combined matrix produced a well-resolved consensus tree with strong nodal support (Figure 1A). Monophyly of the Perittopinae was robustly supported, marking the first comprehensive cladistic analysis based on complete species-level representation within the subfamily. All four newly established genera (*Indoperittopus* **gen. nov.**, *Pachyperittopus* **gen. nov.**, *Falciperittopus* **gen. nov.**, and *Perittopus*) were retrieved as monophyletic with high branch support. *Indoperittopus* **gen. nov.** was retrieved as sister clade to *Pachyperittopus* **gen. nov.** + *Falciperittopus* **gen. nov.** + *Perittopus.* The next node included the Indian genus *Pachyperittopus* **gen. nov.** and the two Southeast Asian genera (*Falciperittopus* **gen. nov.** and *Perittopus*), with the latter being well-supported as monophyletic. The MP-derived phylogenetic relationships based on the combined dataset produced an identical topology, confirming the monophyly of all four genera. The intergeneric relationships were consistently resolved as (*Indoperittopus* **gen. nov.** + (*Pachyperittopus* **gen. nov.** + (*Falciperittopus* **gen. nov.** + *Perittopus*))) (Figure 1A).

Divergence time estimation

The reconstructed chronogram (Figure 1A) indicated that

Perittopinae diversification commenced during the middle Paleocene, with the establishment of the basal clade containing the genus *Indoperittopus* **gen. nov.** dated to approximately 58.1 Ma (95% HPD 47.4–69.1 Ma; Figure 1). Divergence between *Pachyperittopus* **gen. nov.** and the clade (*Falciperittopus* **gen. nov.** + *Perittopus*) occurred in the late Paleocene, around 55.8 Ma (95% HPD 45.2–67.0 Ma; Figure 1A). Subsequent diversification within *Perittopus* began during the Eocene at approximately 52.9 Ma (95% HPD 42.8–63.5 Ma; Figure 1A). The alignment between diversification times and tectonic chronology (Wu et al., 2023) suggests that the Indian-Eurasian plate collision played a significant role in the early radiation of Perittopinae lineages.

Diversification rate analysis

BAMM-based phylorate plots revealed considerable heterogeneity in diversification rates across the Perittopinae phylogenetic tree (Figure 1A). Elevated diversification rates were concentrated in the early evolutionary history of the group, with sustained high rates during the establishment of all four genera until the early Eocene, around 47.8 Ma (95% HPD 38.1–58.2 Ma). Rate-through-time plots indicated a gradual decline in speciation and net diversification rates following this initial phase, while extinction rates remained relatively stable throughout (Supplementary Figure S3). Mapping these rates onto the phylogeny highlighted a concentration of diversification during the period corresponding to the early stages of the India-Eurasia collision (Figure 1A). Although BAMM did not detect significant shifts among specific lineages, branch-specific rate analysis based on the ClaDS2 model identified distinct differences in speciation rates among clades. In particular, lineages within *Perittopus*, especially those distributed across the Indo-China Peninsula, exhibited notably higher speciation rates (Figure 1B; Supplementary Figure S4). These results support a high diversification rate phase during the initial emergence of Perittopinae genera, aligning temporally with the onset of the Indian plate collision.

Ancestral range estimation

Partitioned model selection identified “Step-stone” DEC+J and DIVALIKE as the best-supported frameworks within the J-incorporated and J-excluded model sets (ΔAIC>2, Supplementary Table S8). Under the DEC+J model, the ancestral range of Perittopinae was inferred to lie within southern India and Sri Lanka (Area A), whereas DIVALIKE reconstructed a composite origin spanning southern India and the southern Sunda region (Area AC) (Figure 2; Supplementary Figure S5). Early diversification was centered in southern India and Sri Lanka (Figure 2), with lineage expansion into the northern Sunda Shelf regions by 55.8 Ma (95% HPD 45.2–67.0 Ma), followed by southern Sunda Shelf colonization around 52.9 Ma (95% HPD 42.8–63.5 Ma). A later northward expansion from the southern Sunda Shelf during the early Miocene (21.5 Ma; 95% HPD 14.8–28.9 Ma) led to the radiation of *Perittopus* across the Indo-China Peninsula. Together, these reconstructions strongly support a southern Indian origin as a biogeographically plausible hypothesis, though alternative AC-area origins remain evolutionarily tenable under different model parameterizations (Figure 2).

Taxonomy

Perittopinae China & Usinger, 1949

Type genus: *Perittopus* Fieber, 1860.

Included genera: *Perittopus* Fieber, 1860, *Indoperittopus* **gen. nov.**, *Pachyperittopus* **gen. nov.**, and *Falciperittopus* **gen. nov.** (Figure 3).

Diagnosis: Medium-sized (2.7–4.6 mm), relatively stout. Sexual dimorphism present, but sexes in most species subequal in size and shape. Apterous (usually more common) and macropterous morphs present. Ground color bright red to orange, some species with various black marks. Forewing of macropterous morph usually black, anterior margin of forewing pale orange in some species. Pilosity various, especially species-specific pilosity on posterior part of abdomen of apterous females. Head relatively small, deflected. Compound eyes semispherical, posteriorly adjacent to pronotum. Ocelli absent. Antenna relatively short and stout; antennal segment I longest. Rostrum relatively long, approximately reaching median part of mesosternum; segment III of rostrum longest. Pronotum of apterous morph long, variable, covering entire mesonotum, and metanotum at least medially. Pronotum of macropterous morph very broad, with distinct humeral angles. Ventral hind margin of head as well as anterior margin of prosternum with or without black spiculae. Legs relatively stout, especially femora; profemur of male usually weakly incrassate; protibia of male with grasping comb (lacking in female); tarsal formula 2-3-3; tarsi of foreleg short and incrassate, tarsi of middle and hind legs long and slender. Forewing with two closed cells formed by thick veins on corium; distal part membranous. Abdominal mediotergites not fused. Mediotergite I laterally separated with laterotergites I. Dorsal hind margin of abdominal segment VIII of male deeply concave. Pygophore and proctiger small and simple. Parameres symmetrical, with various modifications within different genera. Gonocoxae of female simple, plate-like, concealed by abdominal segment VII. Proctiger of female small, directed posteriad or ventrad.

Distribution: From Sri Lanka and southern India to Southeast Asia, with extension into southeast China.

Key to genera of Perittopinae

1) Ground color dark yellow to orange, all species with black marks on thorax and abdomen. Ventral hind margin of head and anterior margin of prosternum without black spiculae. Species from southern India. Female: Proctiger elongate, directed ventrad. Male: Paramere slightly curved, occasionally with subapical tooth-like process or tubercle (Figure 4U–X)..... ..... **2**

1.1) Ground color orange to brownish-red, few species with black marks on thorax and abdomen. Ventral hind margin of head and anterior margin of prosternum with several black spiculae (except *Perittopus ceylanicus*) (Figure 5C–D). Female: Proctiger short, directed posteriad. Male: Paramere strongly curved or helicoid **3**

2) Abdomen extremely short and stout (Figure 3J–K; Figure 4F). Female: Connexiva V–VII and mediotergites VII–VIII without conspicuous pilosity (Figure 4F). Male: Paramere relatively slender, strongly tapering, subapical part with tooth-like process (Figure 4T, Y) .... ***Pachyperittopus* gen. nov.**

2.1) Abdomen relatively slender, convergent (Figure 3A–I; Figure 4A–E). Female: Connexiva V–VII or VI–VII and mediotergites VII or VIII with dense, long, black pilosity (Figure 4A–E). Male: Paramere short and stout, subapical part with or without small tooth or round tubercle (Figure 4P–S, U–X) ..... ***Indoperittopus* gen. nov.**

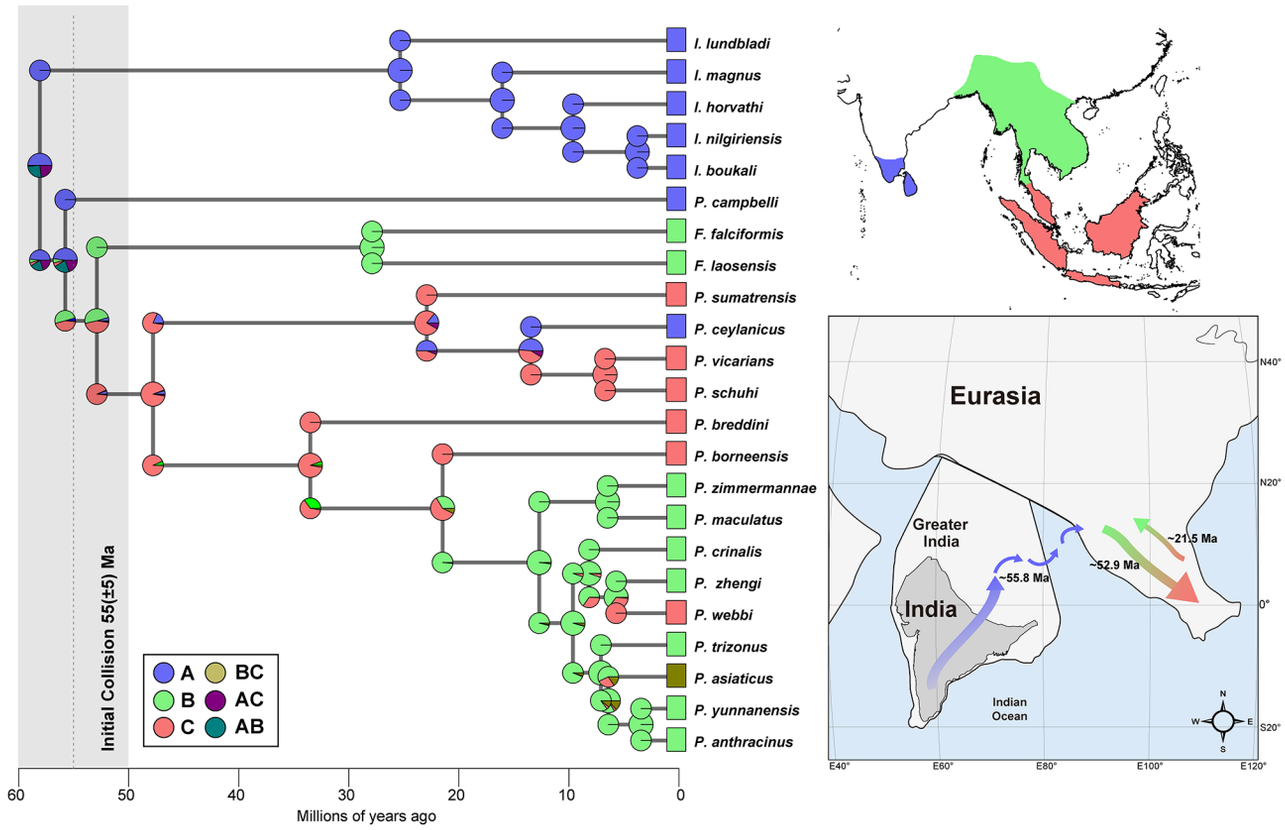

Figure 2 Ancestral range estimation for Perittopinae

Ancestral distributions were inferred using the DEC+J model within the "Step-stone" biogeographic framework, implemented in the BioGeoBEARS package. Terminal node pie charts indicate present-day distributions; internal node pie charts represent reconstructed ancestral ranges. "A" represents South India and Sri Lanka; "B" represents Southwest China and Indo-China Peninsula; "C" represents Malaya and islands of Southeast Asia. Schematic map displays hypothetical dispersal model during India-Eurasia collision, adapted from Figure 4 of "Paleogene India-Eurasia Collision Constrained by Observed Plate Rotation" (Wu et al., 2023).

3) Hind margin of postclypeus almost reaches hind margin of head (Figure 5E–F). Male: Protibial grasping comb of male short, less than 0.24 times protibial length (Figure 5G–H). Paramere slender, strongly curved, forming distal falciform part (Figure 5O–R) ..... ***Falciperittopus* gen. nov.**

3.1) Hind margin of postclypeus distinctly away from hind margin of head. Male: Protibial grasping comb of male long, rarely less than 0.3 times protibial length. Paramere broad, helicoid ..... ***Perittopus***

***Indoperittopus* gen. nov. Zettel & Ehrengruber, 2025**

Type species: *Indoperittopus horvathi* **comb. nov.** (*Perittopus horvathi* Lundblad, 1933)

Included species: *Indoperittopus horvathi* **comb. nov.** (*Perittopus horvathi* Lundblad, 1933), *Indoperittopus boukali* **sp. nov.**, *Indoperittopus nilgiriensis* **sp. nov.**, *Indoperittopus magnus* **sp. nov.**, and *Indoperittopus lundbladi* **sp. nov.**

Diagnosis: Relatively large-sized (3.45–4.50 mm), stout. Ground color dark yellow to reddish-orange. Thorax of both morphs, as well as abdomen of apterous morph with black marks (Figure 3A–I, P–Q; Figure 4A–E, G–J). Pronotum of apterous morph large, posterior lobe distinctly larger than anterior lobe (Figure 4A–E, G–J). Protibial grasping comb of male short, 0.19–0.26 times as long as protibial length (Figure 4K–O). Connexiva V–VII or VI–VII and mediotergites VII or VIII of apterous female with dense, long, black pilosity (Figure 4A–E). Proctiger of female elongate, directed ventrad, with characteristic tuft of short white hairs apically. Paramere of male short and stout, simple, subapical part with or without minute tooth-like process or round tubercle (Figure 4P–S, U–X).

Distribution: Southern India.

Key to species of *Indoperittopus* gen. nov. (apterous morph)

Note: Macropterous morphs are presently only known in *Indoperittopus horvathi* **comb. nov.** and *Indoperittopus boukali* **sp. nov.**

1) Females **2**

1.1) Males (male of *Indoperittopus lundbladi* **sp. nov.** is unknown) **6**

2) Lateral part of mediotergites III–V and sometimes mediotergite VI distinctly black; median part of mediotergite II without distinct black mark (Figure 4A, B). Connexiva IV–VI predominately black or infuscated. Posterior part of connexival margin thin. Gonocoxae dorsally with dense, black pilosity.....**3**

2.1) Mediotergites IV–VI pale yellow to orange; median parts of mediotergite II and sometimes mediotergite III with black mark (Figure 4C–E). Connexiva IV–VI pale yellow to orange. Posterior part of connexival margin thickened. Gonocoxae without such pilosity **4**

3) Head dorsally blackish-brown (Figure 4A). Lateral parts of mediotergites III–VI with distinct black pilosity. Inner part of connexivum V with long, black pilosity, as on connexivum VI..... ..... ***Indoperittopus boukali* sp. nov.**

3.1) Head dorsally yellow (Figure 4B). Lateral parts of

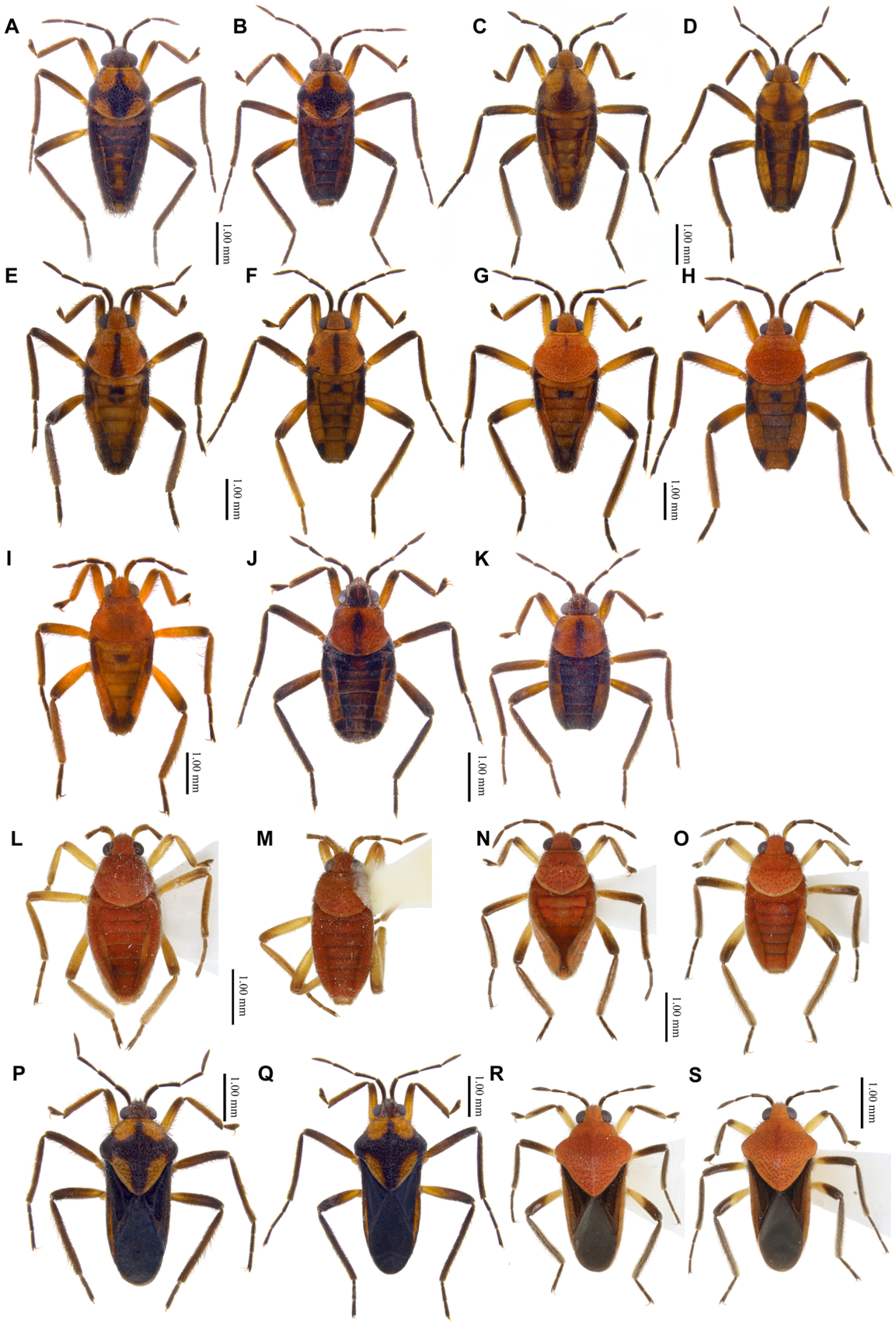

Figure 3 Habitus of *Indoperittopus* gen. nov., *Pachyperittopus* gen. nov. and *Falciperittopus* gen. nov. species

A–O: Apterous form; P, Q: Macropterous form. A, C, E, G, I, J, L, N, R: Female; B, D, F, H, K, M, O, P, Q, S: Male. A, B, P: *Indoperittopus boukali* sp. nov.; C, D: *Indoperittopus nilgiriensis* sp. nov.; E, F, Q: *Indoperittopus horvathi* comb. nov.; G, H: *Indoperittopus magnus* sp. nov.; I: *Indoperittopus lundbladi* sp. nov.; J, K: *Pachyperittopus campbelli* comb. nov.; L, M: *Falciperittopus falciformis* comb. nov.; N, O, R, S: *Falciperittopus laosensis* comb. nov. Photos by Herbert Zettel, Katharina Ehrengruber, Zezhong Jin, and Mu Qiao.

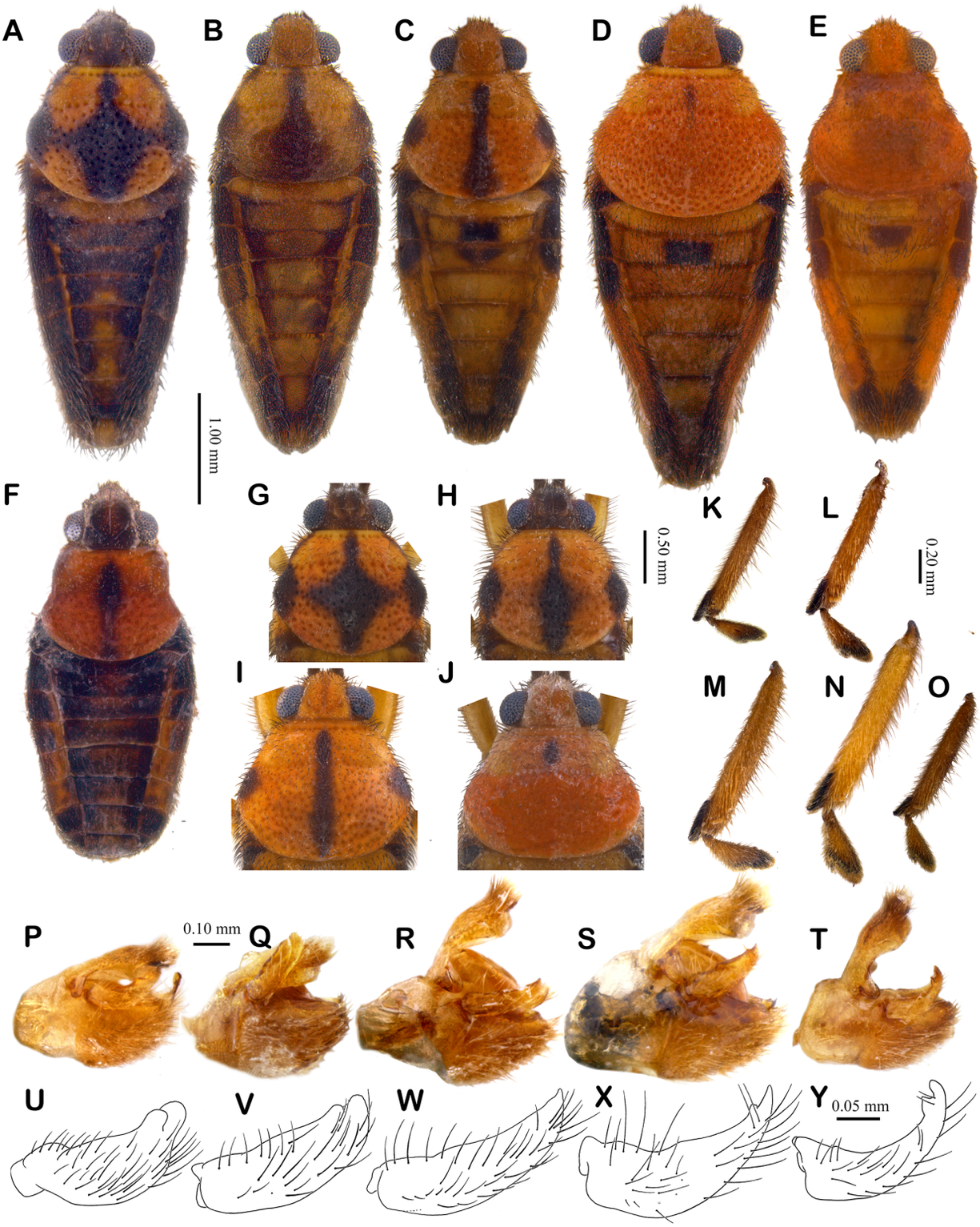

Figure 4 Structural details of *Indoperittopus* spp. and *Pachyperittopus campbelli* comb. nov.

A–F: Body details of apterous female. A: *Indoperittopus boukali* sp. nov.; B: *Indoperittopus nilgiriensis* sp. nov.; C: *Indoperittopus horvathi* comb. nov.; D: *Indoperittopus magnus* sp. nov.; E: *Indoperittopus lundbladi* sp. nov.; F: *Pachyperittopus campbelli* comb. nov. G–J: Variations in color patterns of pronotum of apterous morph. G–H: *Indoperittopus boukali* sp. nov.; I, J: *Indoperittopus magnus* sp. nov. K–O: Protibia and protarsus of male. K: *Indoperittopus boukali* sp. nov.; L: *Indoperittopus nilgiriensis* sp. nov.; M: *Indoperittopus horvathi* comb. nov.; N: *Indoperittopus magnus* sp. nov.; O: *Pachyperittopus campbelli* comb. nov. P–T: Genital capsules of male (in dry condition). P: *Indoperittopus boukali* sp. nov.; Q: *Indoperittopus nilgiriensis* sp. nov.; R: *Indoperittopus horvathi* comb. nov.; S: *Indoperittopus magnus* sp. nov.; T: *Pachyperittopus campbelli* comb. nov. U–Y: Line drawings of left parameres of male in external view. U: *Indoperittopus boukali* sp. nov.; V: *Indoperittopus nilgiriensis* sp. nov.; W: *Indoperittopus horvathi* comb. nov.; X: *Indoperittopus magnus* sp. nov.; Y: *Pachyperittopus campbelli* comb. nov. Photos by Herbert Zettel and Katharina Ehrengruber.

mediotergites III–VI with very short, pale pilosity. Inner part of connexivum V without long pilosity .... ***Indoperittopus nilgiriensis* sp. nov.**

4) Basal part of antennal segment I, meso- and metatibia yellowish-brown (Figure 3I). Median part of pronotum without black stripe or spot (Figure 4E). Brush of black setae on connexivum VII more developed than that on connexivum VI .... ***Indoperittopus lundbladi* sp. nov.**

4.1) Antennal segment I, meso- and metatibia completely blackish-brown (Figure 3E, G). Median part of pronotum with black stripe or spot (Figure 4C, D). Brush of black setae on connexiva VI–VII similarly developed **5**

5) Large and stout species, body length 4.12–4.49 mm, pronotum width 1.61–1.76 mm. Pronotum usually without black humeral corners and rarely with distinct black midline (Figure 4D). Gonocoxae with long, black setae .... ***Indoperittopus magnus* sp. nov.**

5.1) Relatively small and slender species, body length 3.76–4.12 mm, pronotum width 1.42–1.51 mm. Pronotum always with black humeral corners and complete black midline (Figure 4C). Gonocoxae with single long seta .... ***Indoperittopus horvathi* comb. nov.**

6) Mediotergites II–VII laterally or almost black (Figure 3B, D). Subapical part of paramere with tubercle (Figure 4P, Q, U, V) **7**

6.1) Mediotergites II–VII laterally not infuscated (Figure 3H) or only mediotergites IV–VI slightly laterally infuscated (Figure 3F). Subapical part of paramere simple, or with minute tooth-like process (Figure 4R, S, W–X) **8**

7) Head dorsally yellow (Figure 3D). Apical part of paramere broadly rounded (Figure 4Q, V) .... ***Indoperittopus nilgiriensis* sp. nov.**

7.1) Head dorsally black (Figure 3B). Apical part of paramere more narrowly rounded (Figure 4P, U) ....***Indoperittopus boukali* sp. nov.**

8) Large and stout species, body length 4.12–4.32 mm. Subapical part of paramere with minute tooth-like process (Figure 4S, X) ..... .***Indoperittopus magnus* sp. nov.**

8.1) Relatively small and slender species, body length 2.80–3.95 mm. Subapical part of paramere simple (Figure 4R, W) ..... .***Indoperittopus horvathi* comb. nov.**

Species of *Indoperittopus* gen. nov.

***Indoperittopus boukali* sp. nov. Zettel & Ehrengruber, 2025**
(Figure 3A, B, P; Figure 4A, G, H, K, P, U)

Holotype (apterous female): "INDIA: Tamil Nadu, 25.1.1999\ Shevaroy Hills, Yercaud\ Kiliyur Falls env.\ N11°47', E78°12', 1 400 m\ leg. D. Boukal (84)" (NHMW); paratypes: 18 apterous females, 10 apterous males, one macropterous male, same label data as for holotype (NHMW); three macropterous females, four macropterous males, "INDIA: Tamil Nadu, 25.1.1999\ Shevaroy Hills, Yercaud\ Kiliyur Falls env.\ N11°47', E78°12', 1 400 m\ leg. D. Boukal (85)" (NHMW); one apterous female, 120 macropterous females, 93 macropterous males; "INDIA: Tamil Nadu, Palni Hills\ Kodaikanal-Batlagundu Rd.\ Macur env., 1 200 m, N10°16' \ E77°35', 16.1.1999\ leg. D. S. Boukal (68); 50 apterous females, 34 apterous males, 42 macropterous females, 34 macropterous males, "S. INDIA, TAMIL NADU, 1997\ 17.-22.V., 15 km SE Kotagiri\ N11°22', E76°56', Kunchappanai\ Dembicky & Pacholatko leg". (NHMW, NHMS, ZMUC); one female macropterous "SOUTH INDIA\ Yercaud\ 24.IV.1962\ G.J. Spencer", "Brit. Mus.\ 1964–694" (BMNH).

Diagnosis: Medium-sized (3.46–4.20 mm), stout. Ground color yellowish-orange. Thorax of both morphs with large, black, cross-shaped mark (Figure 3A, B, P). Pronotum of apterous morph large, posterior lobe distinctly larger than anterior lobe (Figure 3A, B). Protibial grasping comb of male short, 0.19–0.24 times as long as protibial length (Figure 4K). Abdomen of apterous morph with black marks or infuscated. In apterous female, mediotergites I–III entirely covered with long setae; mediotergites IV–V (VI) laterally with long, black, posteriorly directed setae; posterior part of connexivum V and connexiva VI–VII with dense, long, black pilosity (Figure 4A). Proctiger of female narrow, directed ventrad, apical part with brush of short white setae. Gonocoxae of female dorsolaterally with dense, black pilosity. Paramere of male short and stout, simple, subapical part with rounded tubercle (Figure 4P, U).

Comparative notes: Apterous morphs of *Indoperittopus boukali* **sp. nov.** can be easily distinguished based on a combination of the following characters: head blackish-brown; pronotum with large, black, cross-shaped mark (Figures 3A, B, 4A, G, H). Distinct black lateral parts of mediotergites are present only in *Indoperittopus boukali* **sp. nov.** (darker and broader) and *Indoperittopus nilgiriensis* **sp. nov.** In contrast, macropterous morphs of *Indoperittopus boukali* **sp. nov.** and *Indoperittopus horvathi* **comb. nov.** are more difficult to differentiate (Figure 3P, Q). Compared to *Indoperittopus boukali* **sp. nov.**, males of *Indoperittopus horvathi* **comb. nov.** can be recognized by a more acute paramere apex (Figure 4U vs. W). Macropterous females of *Indoperittopus boukali* **sp. nov.** and *Indoperittopus horvathi* **comb. nov.** could not be readily separated, in the few available specimens of *Indoperittopus horvathi* **comb. nov.** tends to have pale lateral abdominal surfaces and connexival margins, while *Indoperittopus boukali* **sp. nov.** exhibits high color variability, often, but not consistently, with infuscated connexival margins.

Description of apterous female

Measurements (mm): Holotype: Body length 3.58; maximum body width (at metapleura) 1.4. Head width 0.81. Pronotum length 1.14, width 1.37. Lengths of antennal segments: 0.48+0.44+0.48+0.54. Lengths of leg segments: profemur 0.96, protibia 0.98, protarsus 0.05+0.36, mesofemur 1.24, mesotibia 1.43, mesotarsus 0.28+0.36+0.28, metafemur 1.66, metatibia 1.81, metatarsus 0.1+0.31+0.36. Paratypes *(n*=9): Body length 3.58–3.87; maximum body width (at metapleura) 1.45–1.58. Head width 0.81–0.84. Pronotum length 1.15–1.23, width 1.43–1.56.

Color (Figures 3A, P, 4A): Ground color yellow. Head dorsally and partly laterally blackish-brown. Antenna blackish-brown. Pronotum yellowish-orange, with black midline, posteriorly widened, humeri black, in most specimens, connecting to form cross-shaped mark (in lighter specimens, see Figure 4G, H); lateral parts of pronotum with narrow black lines running from black humeri to anterior lobes. Legs yellowish-brown; distal parts of femur, all parts of meso- and metatibia, and all parts of tarsi blackish-brown; protibia pale brown. Lateral parts of mediotergites black, in some specimens anterior mediotergites also infuscated in middle (Figure 4A). Connexiva entirely black, rarely with anterior connexiva mesally pale. Margins of abdominal sterna with black dorsal margin and narrow line along middle, sometimes more extended.

Structures: Body fusiform. Ventral hind margin of head

without black spiculae. Pronotum wide, with weakly developed humeri, posterior pronotal lobe wider than anterior lobe (Figure 4A, G, H), posteromedian margin of pronotum overlapping up to basal half of mediotergite I (Figure 4A); lateral constriction between anterior and posterior lobe not developed; lateral sides with long, black setae. Anterior margin of prosternum without black spiculae. Mediotergites I–III entirely covered with long setae; mediotergites IV–V (VI) laterally with long, black, posteriorly directed setae; hind margins of mediotergite VII and VIII with rows of setae (Figure 4A); mediotergite VIII straight, posteriorly directed. Anterior parts of connexival margins slightly convex, posterior parts straightly convergent, hardly widened posteriorly; smallest distance between connexiva at apex of segment VII (without setae), more than three times connexival width; connexiva II–IV and anterior part of connexivum V with dense, black, posteriorly directed pilosity; posterior part of connexivum V and connexiva VI–VII with very long, black, posteriorly directed pilosity (Figure 4A). Sterna laterally with scattered, long, black, posteriorly directed setae; posterior corner of sternum VII (in lateral view) forming blunt angle. Proctiger narrow, directed ventrad, apical part with brush of short white setae. Gonocoxae narrowly exposed, partly withdrawn in sternum VII, dorsolaterally with black setae almost as long as those on mediotergite VIII.

Description of apterous male

Measurements (mm): Paratypes (*n*=10): Body length 3.46–3.75; maximum body width (at metapleura) 1.32–1.45. Head width 0.79–0.83. Pronotum length 1.08–1.21, width 1.33–1.43. Protibia length 1.02–1.10; protibial comb length 0.21–0.25; comb index 0.20–0.24.

Color (Figure 3B): Similar to apterous female with some exceptions. Abdominal mediotergites almost entirely infuscated.

Structures: Similar to apterous female with some exceptions. Profemur slightly incrassate, length about five times width; protibia with short grasping comb (Figure 4K). Abdomen slender, ovate. All mediotergites and connexiva bear black setae, longest setae located on lateral parts of mediotergites I–VII and in transverse rows on mediotergites II–IV. Paramere (Figure 4P, U) small and stout, moderately widened in middle, with rounded apex and subapical tubercle.

Description of macropterous female

Measurements (mm) (*n*=10): Body length 3.74–4.20; maximum body width (at pronotal humeri) 1.67–1.84. Head width 0.83–0.88. Pronotum length 1.56–1.80, width 1.67–1.84.

Color (Figure 3P): Similar to apterous with some exceptions. Pronotum with broader cross-shaped mark, humeri broadly black. Forewings black (Figure 3P). Connexival and sternal margins often infuscated, with dark stripe at margins of sterna in many specimens.

Structures: Similar to apterous female with some exceptions. Pronotum (Figure 3P) with strongly developed humeri, posterior lobe of pronotum much longer than anterior lobe. Forewing with two basal cells; veins (except costal vein) relatively slender, covering with short, black pilosity (Figure 3P). Connexival margins weakly convex except apical parts, laterally surpassing costal vein except on connexivum VII (Figure 3P).

Description of macropterous male

Measurements (mm) (*n*=10): Body length 3.65–4.07; maximum body width (at pronotal humeri) 1.62–1.74. Head width 0.77–0.81. Pronotum length 1.56–1.74. Protibia length 0.99–1.13; protibial comb length 0.20–0.23; comb index 0.19–0.23.

Color: Similar to macropterous female, but connexival margins not infuscated in all specimens.

Structures: Pronotum, forewing, and connexival margins similar to macropterous female. Foreleg and genital segments as in apterous male.

Distribution: Southern India (Tamil Nadu).

Etymology: This new species is named after one of its discoverers, the coleopterist Dr. David Boukal.

***Indoperittopus nilgiriensis* sp. nov. Zettel & Ehrengruber, 2025** (Figures 3C, D, 4B, L, Q, V)

Holotype (apterous female; NHMW): India, Tamil Nadu, Nilgiri Hills, Thaishola\ N11°14', E76°37', 2 100 m a.s.l., 23.I.1999, leg. D. Boukal (#81). Paratypes (NHMW): one apterous female, two apterous males, same locality data as for holotype; one apterous male, India, Tamil Nadu, Nilgiri Hills, 5 km E Kundah, N11°18', E76°40', 1 900 m a.s.l., 23.I.1999, leg. D. Boukal (#80).

Diagnosis: Medium-sized (3.58–3.99), stout. Ground color yellow. Thorax of both sexes with black midline, posteriorly widened and diffuse; humeri black (Figures 3C, D, 4B). Pronotum of apterous morph large, posterior lobe distinctly larger than anterior lobe (Figures 3C, D, 4B). Protibial grasping comb of male short, 0.23–0.25 times as long as protibial length (Figure 4L). Lateral parts of abdominal mediotergites and connexiva (except connexivum V of female and connexiva IV–VI of male) of apterous morph with black marks or infuscated (Figures 3C, D, 4B). In apterous female, mediotergites I–II covered with long setae; hind margin of mediotergite VII with brush of dense, long, posteriorly directed setae (Figure 4B); posterior part of connexiva VI and VII with very long, black, posteriorly directed pilosity (Figure 4B). Proctiger of female narrow, directed ventrad. Gonocoxae of female dorsoapically with tuft of short black setae. Paramere of male short and stout, simple, subapical part with small rounded tubercle (Figure 4Q, V).

Comparative notes: *Indoperittopus nilgiriensis* **sp. nov.** is closely related to *Indoperittopus boukali* **sp. nov.** but can be distinguished by a combination of the following characters: head yellow; dark midline of pronotum not connected with black humeral corners (Figures 3C, D, 4B); infuscation on connexiva IV–VI absent; abdomen of apterous female pilosity; paramere with rounded apex in male (Figure 4Q, V).

Description of apterous female

Measurements (mm): Holotype: Body length 3.99; maximum body width (at metapleura) 1.55. Head width 0.88. Pronotum length 1.08, width 1.43. Lengths of antennal segments: 0.58+0.45+0.48+0.48. Lengths of leg segments: profemur 1.05, protibia 1.02, protarsus 0.07+0.39, mesofemur 1.3, mesotibia 1.5, mesotarsus 0.32+0.37+0.45, metafemur 1.51, metatibia 1.97, metatarsus 0.13+0.3+0.45. Paratype (*n*=1): Body length 3.99; maximum body width (at metapleura) 1.55. Head width 0.88. Pronotum length 1.05, width 1.46.

Color (Figure 3C): Ground color yellow. Head not infuscated. Antenna blackish-brown. Pronotum yellow, with black midline, posteriorly widened and diffuse; humeri black (Figures 3C, 4B); lateral parts of pronotum with narrow black lines running from humeri to anterior lobes. Legs yellow, distal parts of femur, all parts of meso- and metatibia, and all parts of tarsi

brown. Mediotergites pale in middle, but lateral parts of mediotergites III–V black (Figure 4B). Connexiva entirely black, except connexivum V (Figure 4B). Margins of abdominal sternites II, VI, and VII black.

Structures: Body fusiform. Ventral hind margin of head without black spiculae. Pronotum wide, with weakly developed humeri, posterior pronotal lobe wider than anterior lobe (Figures 3C, 4B), posteromedian margin of pronotum not overlapping basal part of mediotergite I (Figure 4B); lateral constriction between anterior and posterior lobe not developed; lateral sides with long, black setae. Anterior margin of prosternum without black spiculae. Mediotergites I–II covered with some long setae; mediotergites III–V laterally with very short, pale, inconspicuous pilosity; hind margin of mediotergite VII with brush of dense, long, posteriorly directed setae (Figure 4B); mediotergite VIII straight, posteriorly directed, posteriorly with inconspicuous pale pilosity. Anterior parts of connexival margins slightly convex, posterior parts convergent, slightly concave, hardly widened posteriorly; smallest distance between connexiva at apex of segment VII (without setae), more than two times connexival width; connexivum II and lateral half of connexiva III–IV with dense, black, posteriorly directed pilosity; connexivum V and basal part of connexivum VI with much shorter, pale pilosity, other parts of connexiva VI and VII with very long, black, posteriorly directed pilosity (Figure 4B). Sterna laterally with scattered, long, black, posteriorly directed setae; posterior corner of sternum VII (in lateral view) forming blunt angle. Proctiger narrow, directed ventrad, apical part with brush of short, white setae. Gonocoxae narrowly exposed, partly withdrawn in sternum VII, with short pilosity and dorsoapically with tuft of short black setae.

Description of apterous male

Measurements (mm): Paratypes (*n*=3): Body length 3.58–3.79; maximum body width (at metapleura) 1.27–1.46. Head width 0.83–0.88. Pronotum length 0.99–1.07, width 1.25–1.42. Protibia length 1.03–1.06; protibial comb length 0.25–0.26; comb index 0.23–0.25.

Color (Figure 3D): Similar to apterous female with some exceptions. Abdominal mediotergites II–VII laterally infuscated and connexiva IV and VI not infuscated.

Structures: Similar to apterous female with some exceptions. Profemur slightly incrassate, length about five times width; protibia with short grasping comb (Figure 4L). Abdomen slender, ovate. All mediotergites and connexiva bear black setae, longest setae located on lateral parts of mediotergites I–VII. Paramere (Figure 4Q, V) small and stout, moderately widened in middle, with broadly rounded apex and small round subapical tubercle.

Macropterous morph: Unknown.

Distribution: India: Tamil Nadu (Nilgiri Hills).

Etymology: Named after its montane distribution in the Nilgiri Hills.

***Indoperittopus horvathi* comb. nov.** (*Perittopus horvathi* Lundblad, 1933) (Figures 3E, F, Q, 4C, M, R, W)

Syntypes (one apterous female in NHMS, one macropterous female in MTMB): “INDE.MERe.\ TRICHINOPOLY. [Tiruchchirappalli]\ Jos.Debreuil”. “Perittopus\ horvathi Lundbl.\ det. O. Lundblad”. Further material: 15 apterous males, 10 apterous females, three macropterous males, two macropterous females, India, Tamil Nadu, Palni Hills, near Kodaikanal, Vellagavi, N10°11', E77°29', 900 m a.s.l., 13.I.1999, leg. D. Boukal (#62) (NHMW). five macropterous males, six macropterous females, “Naraikkadu, 2 500–3 000'\ Tinnevelly Dt. [Tirunelveli]\ S. India. 10-III-36\\ B.M.-C.M.\ Expedn to\ S. India. 1936”. (BMNH).

Diagnosis: Medium-sized (3.79–4.12 mm), stout. Ground color light yellowish-orange. Thorax of both apterous sexes with black midline; humeri black (Figures 3E, F, 4C). Pronotum of apterous morph large, posterior lobe distinctly larger than anterior lobe (Figures 3E, F, 4C). Protibial grasping comb of male short, 0.23–0.26 times as long as protibial length (Figure 4M). In apterous female, mediotergites II and III medial with large, square, black marks (Figure 4C); hind margin of mediotergite VI with long, posteriorly directed setae; mediotergite VII with dense brush of very long, black hairs. Connexiva I–III and adjacent parts of sterna black, lateral parts of connexiva VI and VII and adjacent parts of sterna more or less brownish infuscated; narrow midline of connexiva III–IV and most parts of V–VII with long, black, posteriorly directed setae (Figure 4C). In apterous male, black, square mark restricted to mediotergite II (Figure 3F). Lateral parts of mediotergites IV–VI more or less distinctly infuscated, connexivum VII strongly infuscated (Figure 3F). All mediotergites and connexiva uniformly set with long, erect, black setae. Paramere (Figure 4R, W) slender, evenly curved, subapical part without tooth or tubercle, apex acute.

Comparative notes: Apterous morphs of *Indoperittopus horvathi* **comb. nov.** can be easily distinguished by the presence of a black midline and black humeral spots on the pronotum of all specimens. In nearly all apterous females both mediotergites II and III exhibit medial black markings. *Indoperittopus horvathi* **comb. nov.** resembles *Indoperittopus lundbladi* **sp. nov.** in overall body shape and is notably more slender than *Indoperittopus magnus* **sp. nov.**, despite a similar abdominal pilosity in females. In apterous females, the connexival margins are moderately expanded, broader than in *Indoperittopus magnus* **sp. nov.**, but narrower than in *Indoperittopus lundbladi* **sp. nov.** Males are distinguishable from *Indoperittopus magnus* **sp. nov.** based on paramere shape (Figure 4W vs. X). Macropterous females closely resemble those of *Indoperittopus boukali* **sp. nov.** (see comparative notes).

Description of apterous female

Measurements (mm): Syntype: Body length 3.95, maximum body width (at metapleura) 1.61. Head width 0.90. Pronotum length 1.16, width 1.47. Length of antennal segments: 0.61+0.50+0.49+0.57. Lengths of leg segments: profemur 1.05, protibia 1.03, protarsus 0.06+0.44, mesofemur 1.42, mesotibia 1.53, mesotarsus 0.31+0.37+0.45, metafemur 1.60, metatibia 1.85, metatarsus 0.1+0.31+0.49. Measurements of non-type specimens (*n*=9): Body length 3.87–4.12; maximum body width (at metapleura) 1.51–1.61. Head width 0.88–0.92. Pronotum length 1.10–1.23, width 1.42–1.51.

Color (Figure 3E): Ground color light yellowish-orange. Head not infuscated. Antenna blackish-brown. Posterior lobe of pronotum brighter orange; pronotum with black midline; humeri black (Figures 3E, 4C). Legs yellow, distal part of femur, all parts of meso- and metatibia, and all parts of tarsi blackish-brown. Mediotergites II and III, rarely only II, medially with large, square, black marks. Connexiva I–III and adjacent parts of sterna black. Lateral parts of connexiva VI and VII and adjacent parts of sterna more or less brownish infuscated.

Structure: Body fusiform. Ventral hind margin of head without

black spiculae. Pronotum wide, medially indistinctly carinate, with weakly developed humeri, posterior pronotal lobe wider than anterior lobe (Figures 3E, 4C), posteromedian margin of pronotum overlapping basal quarter or one-third part of mediotergite I (Figure 4C); lateral constriction between anterior and posterior lobe not developed; whole surface with long, black setae. Anterior margin of prosternum without black spiculae. Mediotergites I–II covered with short, inconspicuous, yellow pilosity; mediotergites I–V with very scattered, short, black bristles (longest on mediotergites I and II, usually lacking in median parts of mediotergites IV–VI); hind margin of mediotergite VI with long, posteriorly directed setae; mediotergite VII with dense brush of very long, black hairs (Figure 4C); mediotergite VIII straight, posteriorly directed, with dense, thin, brown setae. Anterior parts of connexival margins slightly convex, posterior parts straightly convergent, hardly widened posteriorly; smallest distance between connexiva at apex of segment VII (without setae), approximately 1.5 times connexival width; mesal parts of connexiva III–V hairless (widest part on connexivum IV, occupying more than half of width); connexiva I–II with short, dense, black, posteriorly directed setae, narrow midline of connexiva III–IV and most parts of V–VII with long, black, posteriorly directed setae (Figure 4C). Sterna laterally with some scattered, long, black, posteriorly directed setae; posterior corner of sternum VII (in lateral view) forming very blunt angle. Proctiger narrow, directed ventrad, apical part with brush of short white setae. Gonocoxae narrowly exposed, withdrawn in sternum VII, with short pilosity and single long seta.

Description of apterous male

Measurements (mm) (*n*=10): Body length 3.79–3.95; maximum body width (at metapleura) 1.42–1.53. Head width 0.85–0.89. Pronotum length 1.11–1.21, width 1.38–1.50. Protibia length 1.10–1.20; protibial comb length 0.26–0.28; comb index 0.23–0.26.

Color (Figure 3F): Similar to apterous female with some exceptions. On abdomen, black, square mark restricted to mediotergite II, lateral parts of mediotergites IV–VI more or less distinctly infuscated (Figure 3F); connexiva V and VI not infuscated, connexivum VII more strongly infuscated than in female (Figure 3F).

Structures: Similar to apterous female with some exceptions. Profemur slightly incrassate, length about five times width; protibia with short grasping comb (Figure 4M). Abdomen slender, ovate. All mediotergites and connexiva uniformly set with long, erect, black setae. Paramere (Figure 4R, W) slender, evenly curved, subapical part without tooth or tubercle, apex acute.

Description of macropterous female

Measurements (mm) (*n*=7): Body length 3.93–4.32, width (at pronotal humeri) 1.72–1.90. Head width 0.80–0.88. Pronotum length 1.68–1.85, width 1.72–1.90.

Color (Figure 3Q): Similar to apterous with some exceptions. Head dorsally infuscated. Pronotum with broad cross-shaped mark, humeri broadly black, narrow black lines running from humeri to anterior lobes more or less distinct. Forewings black (Figure 3Q). Protibia darker than in apterous morph. Connexival margins not infuscated.

Structures: Similar to apterous female with some exceptions. Pronotum (Figure 3Q) with strongly developed humeri, posterior lobe of pronotum much longer than anterior lobe. Forewing with two basal cells; veins (except costal vein) relatively slender, covered with short, black pilosity (Figure 3Q). Connexival margins weakly convex except apical parts, laterally surpassing costal vein except on connexivum VII (Figure 3Q). Gonocoxae with several long black hairs.

Description of macropterous male

Measurements (mm) (*n*=8): Body length 3.79–4.49, width (at pronotal humeri) 1.59–1.87. Head width 0.77–0.86. Pronotum length 1.56–1.87, width 1.59–1.87. Protibia length 0.98–1.21; protibial comb length 0.21–0.26; comb index 0.20–0.22.

Color: Similar to macropterous female.

Structures: Pronotum, forewing, and connexival margins similar to macropterous female. Foreleg and genital segments as in apterous male except profemur, very slender, about six times as long as wide.

Distribution: India (Tirunelveli).

Further notes: The macropterous series from the Natural History Museum in London was identified with some reservation due to its provenance from the type locality of *Indoperittopus lundbladi* **sp. nov.** However, the parameres exhibit diagnostic features consistent with *Indoperittopus horvathi* **comb. nov.** and the female coloration differs strongly from *Indoperittopus lundbladi* **sp. nov.**

***Indoperittopus magnus* sp. nov. Zettel & Ehrengruber, 2025 (Figures 3G, H, 4D, E, I, J, N, S, X)**

Holotype (apterous female; NHMW): India, Kerala, 15 km southwest of Munnar, Kallar Valley, N10°02', E76°58', 1 250 m a.s.l., 1–9.V.1997, leg. Dembický & Pacholátko. Paratypes (all apterous; NHMW): three males, three females, same locality data as for holotype; one male, two females, nearby locality, Kallar Valley, N10°03', E76°58', 1 100 m a.s.l., 7.I.1999, leg. D. Boukal (#50); one male, three females, nearby locality, Kallar Valley, N10°03', E76°58–59', 1 100–1 200 m a.s.l., 7–8.I.1999, leg. D. Boukal (#49/52); one male, one female, India, Kerala, 10 km west of Munnar, at road between Peschadu and Mangulam, N10°04', E76°58', 1 100 m a.s.l., 6.I.1999, leg. D. Boukal (#48).

Diagnosis: Large-sized (4.12–4.36), very stout. Ground color light yellowish-orange. Anterior part of pronotum often with more or less infuscated midline. Mediotergite II medially with large, square, black mark (Figures 3G, H, 4D). Laterotergites I–III and VII and adjacent parts of sterna black. Pronotum of apterous morph large, posterior lobe distinctly larger than anterior lobe (Figures 3G, H, 4D). Protibial grasping comb of male short, 0.22–0.25 times as long as protibial length (Figure 4N). In apterous female, hind margin of mediotergite VI with long, posteriorly directed setae; mediotergite VII with brush of dense, very long, black setae (Figure 4D). Median part of connexivum V and most parts of connexiva VI–VII with long, black, posteriorly directed setae (Figure 4D). Proctiger of female narrow, directed ventrad. Gonocoxae of female with short pilosity and some long, thin setae. In apterous male, all mediotergites and connexiva uniformly set with long, erect, black setae (Figure 4D). Paramere (Figure 4S, X) slender, evenly curved, with small subapical process on dorsal margin, apex acute.

Comparative notes: *Indoperittopus magnus* **sp. nov.** is closely related to *Indoperittopus horvathi* **comb. nov.** and *Indoperittopus lundbladi* **sp. nov.** but differs by its consistently larger size. Parameres of *Indoperittopus magnus* **sp. nov.** and *Indoperittopus horvathi* **comb. nov.** differ by a small subapical tooth.

Description of apterous female

Measurements (mm): Holotype: Body length 4.36; maximum body width (at metapleura) 1.82. Head width 0.96. Pronotum length 1.37, width 1.76. Lengths of antennal segments: 0.80+0.65+0.58+0.61. Lengths of leg segments: profemur 1.55, protibia 1.23, protarsus 0.08+0.49, mesofemur 1.59, mesotibia 1.87, mesotarsus 0.39+0.45+0.58, metafemur 3.37, metatibia 2.26, metatarsus 0.14+0.41+0.54. Paratypes (*n*=9): Body length 4.12–4.49; maximum body width (at metapleura) 1.69–1.87. Head width 0.93–0.97. Pronotum length 1.23–1.33, width 1.61–1.76.

Color (Figure 3G): Ground color light yellowish-orange. Head, pronotum, and parts of connexival margins bright orange, but color on two anterolateral parts of pronotum usually yellow. Antenna blackish brown. Anterior part of pronotum often with more or less infuscated midline (Figures 3G, 4D, I, J), in one specimen with distinct spot, rarely diffuse to posterior lobe; humeri of pronotum in one specimen with small black dots (Figure 4I). Legs yellow, distal parts of femur, all parts of meso- and metatibia, and all parts of tarsi blackish-brown. Mediotergite II medially with large, square, black mark (lacking in one specimen). Laterotergites I–III and VII and adjacent parts of sterna black.

Structures: Body fusiform, stout. Ventral hind margin of head without black spiculae. Pronotum wide, with weakly developed humeri, posterior pronotal lobe wider than anterior lobe (Figures 3G, 4D, I, J), posteromedian margin of pronotum overlapping basal quarter or half part of mediotergite I (Figure 4D); lateral constriction between anterior and posterior lobe not developed; whole surface with long, black setae. Anterior margin of prosternum without black spiculae (or rarely with very few). Mediotergites I and II with short, inconspicuous, yellow pilosity; mediotergites I–V with scattered, short, black bristles (longest on mediotergites I and II, usually lacking in median parts of mediotergites IV–VI); hind margin of mediotergite VI with long, posteriorly directed setae; mediotergite VII with brush of dense, very long, black setae (Figure 4D); mediotergite VIII slightly curved ventrad, densely set with thin, brown setae. Anterior parts of connexival margins slightly convex, posterior parts slightly concave; weakly widened posteriorly, smallest distance between connexiva at apex of segment VII (without setae), approximately two times connexival width; mesal parts of connexiva III–VI with hairless parts (widest part on connexivum IV, occupying more than half of width); connexiva I–III with short, dense, black, posteriorly directed setae, median part of connexivum V and most parts of connexiva VI–VII with long, black, posteriorly directed setae (Figure 4D). Sterna laterally with several scattered, long, black, posteriorly directed setae; posterior corner of sternum VII (in lateral view) rounded. Proctiger narrow, directed ventrad, apical part with brush of short white setae. Gonocoxae narrowly exposed, withdrawn in sternum VII, with short pilosity and some long, thin setae.

Description of apterous male

Measurements (mm): Paratypes (*n*=6): Body length 4.12–4.32; maximum body width (at metapleura) 1.59–1.74. Head width 0.93–0.98. Pronotum length 1.27–1.41, width 1.56–1.69. Protibia length 1.30–1.37; protibial comb length 0.30–0.32; comb index 0.22–0.25.

Color (Figure 3H): Similar to apterous female. In two specimens pronotum with almost complete black midline and large black humeral spots.

Structures: Similar to apterous female with some exceptions. Pronotum from anterior margin to humeri less strongly widened. Profemur slightly incrassate, length ca. 4.5 times width, protibia with short grasping comb (Figure 3H). Abdomen slender, ovate. All mediotergites and connexiva uniformly set with long, erect, black setae. Paramere (Figure 4S, X) slender, evenly curved, with small subapical process on dorsal margin, apex acute.

Macropterous morph: Unknown.

Distribution: India: Kerala (Cardamom Hills).

Etymology: Magnus (Latin, adjective) meaning large, referring to the size of the species, which is the largest in this genus.

***Indoperittopus lundbladi* sp. nov. Zettel & Ehrengruber, 2025** (Figures 3I, 4E)

Holotype (apterous female; BMNH): "Naraikkadu, 2 500-3 000'\ Tinnevelly Dt. [=Tirunelveli in Tamil Nadu]\ S. India. 10-III-36\\ B.M.-C.M.\ Expedn to\ S. India. 1936". Paratypes (BMNH, NHMW): three apterous females, same locality data as for holotype.

Diagnosis: Medium-sized (3.70–3.87), stout. Ground color pale yellow. Dorsum of head, pronotum, and parts of connexival margins yellowish-orange; pronotum without dark marks (Figure 3I; Figure 4E). Median part of mediotergite II with dark brown mark (Figures 3I, 4E). Connexiva I–III, connexivum VII, and adjacent parts of sterna black. In apterous female, hind margin of mediotergite VI with long posteriorly directed setae; mediotergite VII with brush of dense, very long, black setae (Figure 4E). Connexiva IV–VI with relatively narrow middle stripe of black hairs, connexivum VII completely covered with brush of dense, long, black, posteriorly directed setae (Figure 4E). Proctiger of female narrow, directed ventrad. Gonocoxae with short pilosity and some long thin setae.

Comparative notes: This species is closely related to *Indoperittopus horvathi* **comb. nov.** and *Indoperittopus magnus* **sp. nov.** but differs from those species by its smaller size, lighter antenna and leg coloration, reduced black dorsal color pattern, more strongly convergent and posteriorly flattened connexiva, and different pilosity on connexiva of apterous female (Figures 3I, 4E). Furthermore, it can be distinguished from *Indoperittopus horvathi* **comb. nov.** by the long pilosity on the gonocoxae of apterous female.

Description of apterous female

Measurements (mm): Holotype: Body length 3.87; maximum body width (at metapleura) 1.61. Head width 0.90. Pronotum length 1.10, width 1.48. Lengths of antennal segments: 0.58+0.49+0.48+0.53. Lengths of leg segments: profemur 1.03, protibia 1.11, protarsus 0.06+0.41, mesofemur 1.39, mesotibia 1.63, mesotarsus 0.31+0.40+0.49, metafemur 1.35, metatibia 1.95, metatarsus 0.09+0.32+0.52. Measurements of paratypes (*n*=3): Body length 3.70–3.87; maximum body width (at metapleura) 1.58–1.61. Head width 0.84–0.90. Pronotum length 1.03–1.14, width 1.43–1.48.

Color (Figures 3I, 4E): Ground color pale yellow. Dorsum of head, pronotum, and parts of connexival margins yellowish-orange; pronotum without dark marks. Antennal segment I yellow, II–IV yellowish-brown. Legs yellow, apical part of femur slightly infuscated, tarsi brown. Median part of mediotergite II with dark brown mark (very indistinct in one specimen). Connexiva I–III, connexivum VII, and adjacent parts of sterna

black (very indistinct in same specimen).

Structures: Body fusiform. Ventral hind margin of head without black spiculae. Pronotum wide, with weakly developed humeri, posterior pronotal lobe wider than anterior lobe (Figures 3I, 4E), posteromedian margin of pronotum not or hardly overlapping basal part of mediotergite I (Figure 4E); lateral constriction between anterior and posterior lobe not developed; whole surface with scattered, long, black bristles, usually absent posteromedially. Anterior margin of prosternum without black spiculae. Mediotergites I–II with scattered long setae (black-marked area of mediotergite II sometimes bearing setal cluster); mediotergites III–V with sparse, short, black bristles; hind margin of mediotergite VI with long posteriorly directed setae; mediotergite VII with brush of dense, very long, black setae (Figure 4E); mediotergite VIII slightly curved ventrad, densely set with thin, brown setae. Anterior parts of connexival margins slightly convex, posterior parts slightly concave (almost straight); connexiva IV–VII very thick; smallest distance between connexiva at apex of segment VII (without setae), subequal or slightly wider than connexival width; mesal parts of connexiva III–VI with broad hairless and impressed parts (occupying about half of width), short and strongly narrowed at connexivum VII; connexiva IV–VI with relatively narrow middle stripe of black hairs, connexivum VII completely covered with brush of dense, long, black, posteriorly directed setae. Sterna with scattered, long, black, posteriorly directed setae; posterior corner of sternum VII (in lateral view) rounded. Proctiger narrow, directed ventrad, apical part with brush of short, white setae. Gonocoxae narrowly exposed, withdrawn in sternum VII, with short pilosity and several long thin setae.

Apterous male and macropterous morph: Unknown.

Distribution: India: Tamil Nadu (Tirunelveli). Elevation on label suggests that the type locality lies along the Agasthyamalai Range.

Etymology: Named in honor of the late Prof. O. Lundblad, whose foundational work on *Perittopus* forms the basis of this revision.

***Pachyperittopus* gen. nov. Zettel, Ehrengruber & Jin, 2025**

Type species: *Pachyperittopus campbelli* **comb. nov.** (*Perittopus campbelli* Lundblad, 1933)

Diagnosis: Medium-sized (2.80–3.46 mm), very stout. Ground color brownish-yellow. Head infuscated. Median part of pronotum with black stripe (Figures 3J, K, 4F). Lateral parts of mediotergites and connexiva largely black (Figure 4F). Pronotum of apterous morph small, posterior lobe slightly larger than anterior lobe (Figures 3J, K, 4F). Protibial grasping comb of male short, about 0.17 times as long as protibial length (Figure 4O). Abdomen very stout, mediotergites and connexiva of apterous female with scatted, short setae, connexiva straightly convergent (Figures 3J, K, 4F). Proctiger of female short, narrow, directed ventrad, apical part with some short setae. Paramere of male slender, slightly curved, strongly tapering towards apex, subapical part with distinct, stout tooth-like process at dorsal margin (Figure 4T, Y).

Distribution: Southern India.

Species of *Pachyperittopus* gen. nov.

Pachyperittopus campbelli **comb. nov.** (Figures 3J, K, 4F, O, T, Y)

Syntype (apterous female): “Kodai Kanal.\ S. India.\ T.V. Campbell”, “Perittopus\ campbelli Lundbl.\ det. Dr. O. Lundblad” (MTMB); two syntypes (apterous female and male, glued on one card) “Kodai Kanal\ S. India\ T.V. Campbell” [in Lundblad’s handwriting], “Cotypus”, Perittopus\ campbelli Lundbl.\ det. O. Lundblad” (NHRS); other material: one male, one female “INDIA: Tamil Nadu, 11.I.1999\ Palni Hills, N10°14', E77°29' \ Kodaikanal, Bear Shola Falls\ 2 100 m, leg. D. Boukal (#58)” (NHMW).

Diagnosis: See diagnosis of *Pachyperittopus* **gen. nov.** Zettel & Ehrengruber, 2025 above.

Comparative notes: This species is highly characteristic. The extremely stout body shape (Figure 3J, K), distribution of pilosity on female connexiva, and subapical part of the male paramere are unique among Perittopinae (Figure 4T, Y).

Description of apterous female

Measurements (mm): Syntype: Body length 3.46; maximum body width (at hind margin of abdominal segment II) 1.66; head width 0.87; pronotum length 1.03, width 1.33. Length of antennal segments: 0.46+0.37+0.41+0.46. Length of leg segments: profemur 0.88, protibia 0.96, protarsus 0.07+0.38, mesofemur 1.23, mesotibia 1.40, mesotarsus 0.29+0.32+0.45, metafemur 1.31, metatibia 1.68, metatarsus 0.09+0.23+0.44. Measurements of non-type specimen (n=1): Body length 3.46, maximum body width 1.55. Head width 0.87. Pronotum length 1.03, width 1.30. Length of antennal segments: 0.45+0.36+0.39+0.50. Length of leg segments: profemur 0.94, protibia 0.95, protarsus 0.06+0.37, mesofemur 1.24, mesotibia 1.45, mesotarsus 0.27+0.41+0.49, metafemur 1.35, metatibia 1.71, metatarsus 0.12+0.25+0.48.

Color (Figure 3J; Figure 4F): Ground color brownish-yellow. Head infuscated, median part darker. Antenna blackish-brown. Pronotum bright orange, with black median stripe and infuscated margins (Figures 3J, 4F). Basal parts of legs yellowish-orange, apical part of profemur, all parts of meso- and metafemur, tibiae, and tarsi blackish-brown. Median parts of mediotergites dark to brown, lateral parts black (Figure 4F). Connexiva I–IV and VII entirely or largely black (Figure 4F). Lateral margins of all sterna with dark stripes.

Structures: Body very stout; posterior part of abdomen slightly narrow. Ventral hind margin of head without black spiculae. Pronotum relatively small, without median carina, with weakly developed humeri, posterior pronotal lobe slightly wider than anterior lobe (Figure 4F), posteromedian margin of pronotum not overlapping basal part of mediotergite I (Figure 4F); lateral constriction between anterior and posterior lobe developed; lateral sides with long, black setae. Anterior margin of prosternum without black spiculae. Mediotergites wide, with scattered, very short setae; width of mediotergite VII about twice as long as length; mediotergite VIII even wider, directed posteriad, slightly curved. Anterior parts of connexival margins slightly convex, posterior parts straightly convergent, not widened at all (Figure 4F); connexiva only with short pilosity laterally. Lateral margins of sterna with stripe of pilosity; setae slightly increasing in length posteriorly. Posterior corner of sternum VII (in lateral view) forming blunt angle. Proctiger narrow and comparatively short, directed ventrad, apical part with several short, white hairs. Gonocoxae widely exposed, plate-like, with short, dense, even pilosity.

Description of apterous male

Measurements (mm): Syntype: Body length 2.80; maximum body width 1.31; head width 0.78; pronotum length 0.89 width 1.12. Length of antennal segments: 0.43+0.35+0.36+0.42. Length of leg segments: profemur 0.86, protibia 0.84, protarsus 0.05+0.33, mesofemur 1.13, mesotibia 1.25,

mesotarsus 0.24+0.26+? (broken), metafemur 1.15, metatibia 1.51, metatarsus 0.10+0.21+0.40. Measurements of none-type specimen (*n*=1): Body length 2.84; maximum body width (at metapleura) 1.29. Head width 0.80. Pronotum length 0.90, width 1.14. Protibia length 0.89; protibial comb length 0.16; comb index 0.17.

Color (Figure 3K): similar to female, but mediotergites almost entirely black and connexiva darker; however, connexivum IV without black mark.

Structures: Similar to apterous female with some exceptions. Pronotum wide, almost square, without lateral constriction. Profemur moderately incrassate, length about four times as long as width, protibial with short grasping comb (Figure 4O). All mediotergites and connexiva uniformly set with long, decumbent, black setae. Paramere slender, slightly curved, strongly tapering towards apex, subapical part with distinct, stout tooth-like process at dorsal margin, apex acute (Figure 4T, Y).

Macropterous morph: Unknown.

Distribution: See above.

***Falciperittopus* gen. nov. Jin, Qiao & Ye, 2025**

Type species: *Falciperittopus falciformis* **comb. nov.** (*Perittopus falciformis* Ye, Chen & Bu, 2013)

Included species: *Falciperittopus falciformis* **comb. nov.** (*Perittopus falciformis* Ye, Chen & Bu, 2013), and *Falciperittopus laosensis* **comb. nov.** (*Perittopus laosensis* Ye & Bu, 2020).

Diagnosis: Small-sized (2.79–3.23 mm) stout. Ground color red, without black marks (Figures 3L–O, R, S, 5A, B). Antenna relatively long, longer than half of body length; postclypeus long, hind margin almost reaching hind margin of head (Figure 5E, F); ventral hind margin of head and anterior margin of prosternum with some short, black spiculae (Figure 5C, D). Pronotum small, posterior pronotal lobe of apterous female slightly wider than anterior lobe (Figure 5A, B). Protibial grasping comb of apterous male short, 0.17–0.23 times as long as protibial length (Figure 5G, H). Connexiva of apterous female obliquely raised, convergent inward (Figure 5A, B); hind part of abdominal segments VI–VIII with dense, short, posteroventrally directed setae. Proctiger of female short, directed posteriad, with several short setae. Genital capsules of male simple, covered with dense setae (Figure 5I–L). Proctiger simple, lateral margin slightly widened in middle (Figure 5M, N). Paramere of male long and slender, with elongate, slender distal falciform part, subapical part with small dilation (Figure 5O–R).

Distribution: China (Yunnan province), Laos.

For descriptions of *Falciperittopus falciformis* **comb. nov.** and *Falciperittopus laosensis* **comb. nov.,** see Ye et al. (2013) and Ye et al. (2020).

DISCUSSION

Phylogeny of Perittopinae

Integrative analyses incorporating morphological and molecular datasets resolved the internal phylogeny of the subfamily Perittopinae with strong support, recovering it as a monophyletic lineage and sister to Veliinae. This relationship mirrors the hypothesis advanced by Andersen (1982), who posited a close affinity between Perittopinae and the genus *Velia* (Veliidae: Veliinae), albeit without empirical evidence at that time. The present findings tentatively support the conclusion of Andersen (1982); however, broader sampling across Veliinae and additional veliid subfamilies such as Rhagoveliinae and Ocelloveliinae remains essential for robust phylogenetic placement.

Within Perittopinae, topological congruence was observed between the phylogenetic tree derived from combined molecular and morphological data and that based on morphological data alone, both resolving: ((*Perittopus*+*Falciperittopus*)+*Pachyperittopus*)+*Indoperittopus*. All genera formed monophyletic clades (Figure 1A). Notably, mitochondrial (PCG_12S16S) and nuclear (18S and 28S) datasets exhibited conflicting topologies for *P. ceylanicus* (Supplementary Figure S2). The mitochondrial matrix weakly supported its affinity with *Indoperittopus* (bootstrap: 51–57), while the nuclear dataset recovered it within *Perittopus*, although on elongated branches. This discordance may reflect mitochondrial introgression associated with secondary contact between the *P. ceylanicus* and *Indoperittopus* lineages during recolonization of Sri Lanka, coupled with limited phylogenetic signal in the conserved nuclear rDNA loci.

The genera *Perittopus* and *Falciperittopus* formed a well-supported sister group positioned terminally within the phylogeny (Figure 1A). Both genera show a ground color ranging from orange to brownish-red, with the ventral hind margin of the head and anterior margin of the prosternum adorned with black spiculae (except in *Perittopus ceylanicus*) (Lundblad, 1933). Males of both genera possess spiral-shaped parameres, with *Falciperittopus* **comb. nov.** further characterized by a markedly curved, falciform distal portion of the paramere (Lundblad, 1933; Ye et al., 2020). In contrast, the newly established genera *Indoperittopus* **comb. nov.** and *Pachyperittopus* **comb. nov.**, both endemic to southern India, occupy basal positions. These genera are distinguished by their dark yellow to orange coloration and consistent black markings on the thorax and abdomen, as well as their slightly curved parameres, occasionally featuring a subapical tooth-like process or tubercle. Despite the morphological resemblance between these two genera, the phylogenetic tree derived from combined molecular and morphological data, as well as that based on morphological data alone, supported *Pachyperittopus* **comb. nov.** as a distinct clade, not forming a sister group with *Indoperittopus* **comb. nov.** *Pachyperittopus* **comb. nov.** is highly distinctive due to its exceptionally stout body shape (Figure 3J, K), unique distribution of pilosity on the female connexiva, and distinctive morphology of the male paramere subapical region, unparalleled within Perittopinae (Figure 4T, Y). In addition, the antennal segment I of the apterous female is short, posterior pronotal lobe of the apterous female is either slightly longer than or isometric with the anterior lobe, and posterior pronotal lobe of the apterous male exhibits similar length characteristics (Lundblad, 1933). The current monotypic status of *Pachyperittopus* **comb. nov.** limits definitive delineation of its diagnostic morphological characters. Further comprehensive comparisons with additional species are needed to clarify its taxonomic boundaries.

Historical biogeography of Perittopinae

Densely sampled taxon coverage enabled temporal and spatial reconstruction of Perittopinae evolution at unparalleled resolution. Divergence dating and ancestral area estimations inferred a Paleocene origin for the lineage, with initial diversification commencing approximately 58.1 Ma (95% HPD

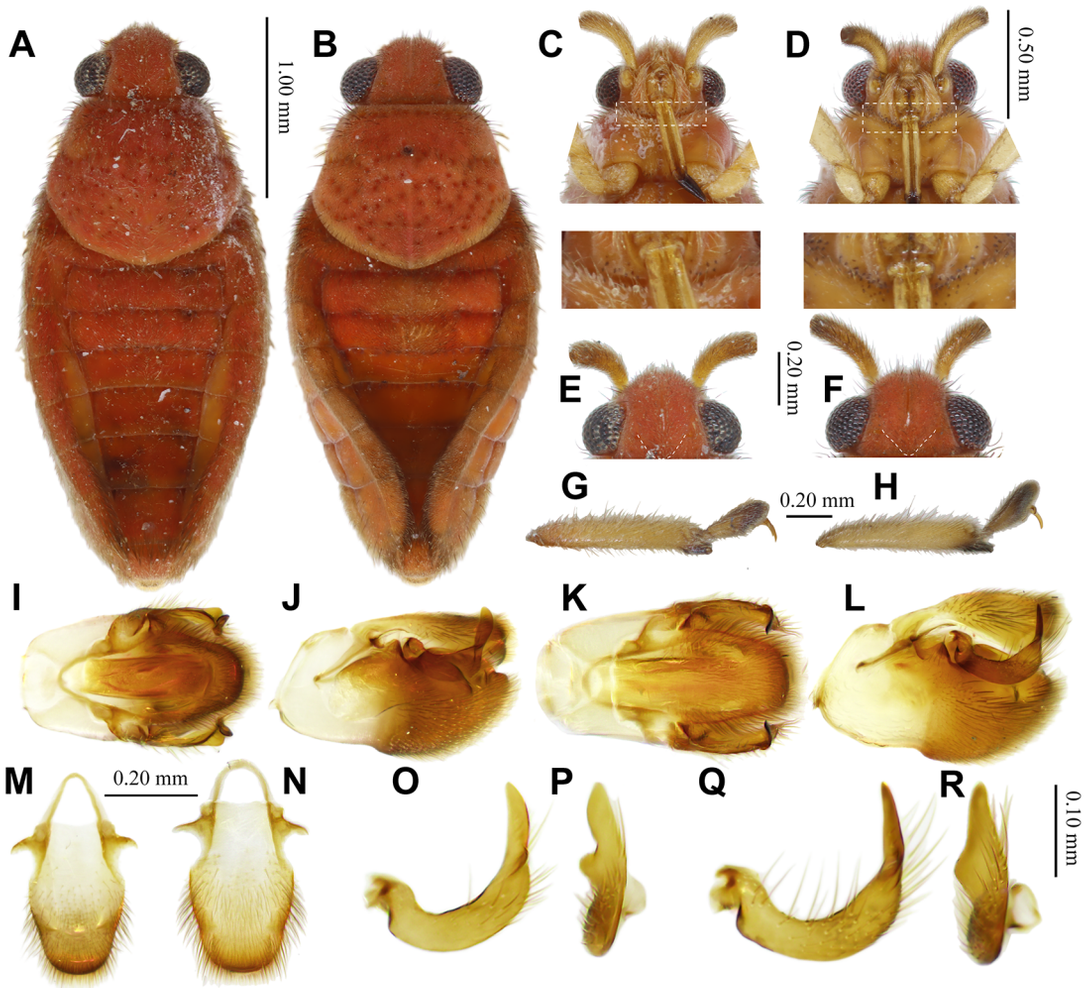

Figure 5 Structural details of *Falciperittopus* spp.

A, C, E, G, I, J, M, O, P: *Falciperittopus falciformis* comb. nov.; B, D, F, H, K, L, N, Q, R: *Falciperittopus laosensis* comb. nov. A, B: Body details of apterous female. C, D: Positions of spiculae. E, F: Head details (showing position of postclypeus hind margin). G, H: Protibia and protarsus of male. I, K: Genital capsules of male in dorsal view. J, L: Genital capsules of male in lateral view. M, N: Proctiger of male in dorsal view. O, Q: Paramere of male in external view. P, R: Paramere of male in perpendicular view. Photos by Zezhong Jin and Mu Qiao.

47.4–69.1 Ma) in the southern Indian subcontinent (Figure 1A). While alternative origin hypotheses—such as composite South India-Sunda patterns inferred under specific model frameworks—remain viable, the southern Indian scenario aligns most closely with molecular dating and paleogeographic constraints. This interpretation, framed cautiously following approaches applied to other putative Gondwanan relicts (Jiang et al., 2022; Liu et al., 2012), remains one of several biogeographically plausible hypotheses.

The inferred timing of origin overlapped with the Deccan volcanic activity that impacted much of peninsular India around 65 Ma. However, recent paleoecological reconstructions suggest elevational refugia persisted in the southern Western Ghat, where cooler microclimates buffered taxa from volcanic disturbances (Bossuyt et al., 2006; Loria & Prendini, 2020). This aligns with the current elevational distribution of extant *Indoperittopus* species, all recorded from 900 to 1 900 m a.s.l. (see Taxonomy section).

Extensive faunal interchange between India and Southeast Asia has been well documented, particularly among invertebrates (Grismer et al., 2016; Klaus et al., 2010; Li et al., 2020; Palmieri et al., 2023; Xu et al., 2021). The dominant framework explaining this biotic exchange between India and Southeast Asia is referred to as the “Biotic ferry” model, which assumes that dispersal was constrained to terrestrial connections between continents due to the limited transoceanic dispersal capacity of many taxa. For example, Klaus et al. (2010) suggested that the proximity of India and Southeast Asia during the Middle Eocene facilitated dispersal of the Asian freshwater crab (Gecarcinucidae) before the final collision between the Indian and Eurasian plates. In contrast, the “Step-stone” model proposes that emergent landmasses such as the Indian Plate functioned as transient dispersal corridors across marine barriers (Yuan et al., 2019). This model is supported in species such as Natatanuran frogs, whereby the Indian plate facilitated overland dispersal across marine barriers and enabled biotic exchange among Africa, Asia, and Madagascar during the Late Cretaceous (Yuan et al., 2019). Employing the step-stone dispersal multipliers from Yuan et al. (2019), our biogeographic analyses identified DEC+J (J-incorporated models) and DIVALIKE (non-J models) as optimal frameworks, supporting a southern Indian origin and a composite South India-Sunda origin hypothesis, respectively. Paleogeographic reconstructions propose early contact between India and western Sundaland during the

Paleocene (Ali & Aitchison, 2008), a scenario supported by multiple phylogeographic studies but lacking definitive geological corroboration (Gorin et al., 2020; Hall, 2013; Klaus et al., 2010; Li et al., 2013). The more widely accepted hypothesis postulates a Paleocene collision between India and an island arc bordering Sundaland, creating a favorable dispersal route even prior to complete continental fusion (Gorin et al., 2020; Hall, 2013; Li et al., 2020; Morley, 2018). Given their semi-aquatic habits and presence of macropterous morphs, it is plausible that ancestral Perittopinae dispersed across this arc to traverse oceanic barriers. Paleoclimatic and topographic reconstructions (Morley, 2018) support an initial dispersal from the Indian subcontinent to eastern Sundaland (Figure 2), excluding the lineage leading to *Indoperittopus* **gen. nov.** and *Pachyperittopus* **gen. nov.** Climatic conditions in eastern Sundaland during the relevant interval mirrored those of southern India (Morley, 2018), providing ecological continuity for colonization. Upon arrival, one lineage underwent *in situ* diversification via founder-effect speciation (Matzke, 2014), giving rise to *Falciperittopus* **gen. nov.** Continued expansion southward subsequently produced the lineage now recognized as *Perittopus*. The accumulation of diversity within *Perittopus* appears to have occurred primarily through *in situ* diversification within Sundaland, consistent with patterns reported for freshwater fish in the region (Sholihah et al., 2021a, 2021b). From the early stages of the India-Asia collision through the Eocene, Perittopinae exhibited elevated speciation rates (Figure 1A; Supplementary Figure S4), likely facilitated by expanding habitat availability, as similarly observed in other species (Gorin et al., 2020; Loria & Prendini, 2020). A noteworthy species is *P. ceylanicus*, which originated in Sundaland but returned to Sri Lanka approximately 13.5 Ma (Figure 2). Comparable “Into India” reversals have been documented in other taxa (Grismer et al., 2016; Li et al., 2013), although the underlying mechanistic drivers of this Late Miocene recolonization remain uncertain due to the absence of paleogeographic or paleoclimatic correlates. This event represents an empirically supported yet unresolved anomaly within an otherwise consistent eastward dispersal narrative. During this period, species migration from mainland Asia into India increased linearly, potentially linked to regional aridification and the decline of perhumid climates in northern Southeast Asia (Klaus et al., 2016). The genus *Perittopus*, which exhibits the highest diversity within the subfamily Perittopinae, is primarily distributed across mainland Southeast Asia, with maximal diversity concentrated in the northern montane regions, particularly the Hengduan Mountains (Figure 1B). This hotspot may reflect the influence of geographic isolation associated with orogenic uplift (Favre et al., 2015; Xing & Ree, 2017). Furthermore, *P. asiaticus* is the most widely distributed species within the subfamily; however, the potential existence of cryptic species within this lineage remains an open question for further investigation.

NOMENCLATURAL ACTS REGISTRATION

The electronic version of this article in portable document format represents a published work according to the International Commission on Zoological Nomenclature (ICZN), and hence the new names contained in the electronic version are effectively published under that Code from the electronic edition alone (see Articles 8.5–8.6 of the Code). This published work and the nomenclatural acts it contains have been registered in ZooBank, the online registration system for the ICZN. The ZooBank LSIDs (Life Science Identifiers) can be resolved and the associated information can be viewed through any standard web browser by appending the LSID to the prefix http://zoobank.org/.

Publication LSID:
urn:lsid:zoobank.org:pub:92DF3382-E4D0-4E43-A1E5-78E762DF534B.
Indoperittopus LSID:
urn:lsid:zoobank.org:act:84D70E22-2450-4433-81CC-46C07F681CF7.
Pachyperittopus LSID:
urn:lsid:zoobank.org:act:43AB1614-AC6F-4F28-9ABD-45AA9572568E.
Indoperittopus boukali LSID:
urn:lsid:zoobank.org:act:8EFA6673-42B7-4768-BE2F-69A9D0D71406.
Indoperittopus lundbladi LSID:
urn:lsid:zoobank.org:act:171C996A-78AB-4A62-B027-DCD4C450B1DD.
Indoperittopus magnus LSID:
urn:lsid:zoobank.org:act:222923F1-ED49-45CF-9F33-98AD7B4F4184.
Indoperittopus nilgiriensis LSID:
urn:lsid:zoobank.org:act:2BDF880C-F141-408A-8C92-0739F656A069.

SCIENTIFIC FIELD SURVEY PERMISSION INFORMATION

Permission for field surveys in the Daweishan National Nature Reserve was granted by the Administration of Daweishan National Nature Reserve; permission for the Huanglianshan National Nature Reserve was granted by the Management Bureau of Huanglianshan National Nature Reserve.

DATA AVAILABILITY

Molecular data were deposited in the Science Data Bank database (10.57760/sciencedb.j00139.00199) and NCBI database (GenBank accession numbers: PV495033–PV495047, PV505127–PV505169, PV520334–PV520510, PV528726–PV528739)

SUPPLEMENTARY DATA

Supplementary data to this article can be found online.

COMPETING INTERESTS

The authors declare that they have no competing interests.

AUTHORS’ CONTRIBUTIONS

M.Q.: Conceptualization; data curation; formal analysis; investigation; methodology; software; validation; writing – original draft. Z.Z.J.: Conceptualization; data curation; methodology; formal analysis; software; visualization; writing–original draft. H.Z.: Conceptualization; Data curation; formal analysis; supervision; visualization; resources; supervision; validation; writing—review and editing. K.E.: Formal analysis; investigation; methodology; visualization. C.L.: Formal analysis; methodology; resources; validation. Z.H.L.: Formal analysis; methodology; validation. Z.Q.L.: Formal analysis; methodology; validation. S.Y.F.: Formal analysis; methodology; validation; resources. W.J.B.: Conceptualization; data curation; resources; supervision; writing—review and editing. Z.Y.: Conceptualization; data curation; investigation; funding acquisition; project administration; software; resources; validation; supervision; visualization; writing—original draft, review and editing. All authors read and approved the final version of the manuscript.

ACKNOWLEDGMENTS

The authors thank Vasarhelyi Tamás (MTMB), Bert Viklund (NHRS), and Michael Webb (BMNH) for the loan of specimens; David Boukal, Luboš Dembický, and Petr Pacholátko for giving specimens to NHMW. The third author is grateful to the late Nils Møller Andersen (formerly ZMUC) for the exchange of specimens and Alice Laciny (NHMW) for her corrections and comments on the early version of the manuscript.

REFERENCES

Aitchison JC, Ali JR, Davis AM. 2007. When and where did India and Asia collide?. *Journal of Geophysical Research: Solid Earth*, **112**(B5): B05423.

Ali JR, Aitchison JC. 2008. Gondwana to Asia: plate tectonics,

paleogeography and the biological connectivity of the Indian sub-continent from the Middle Jurassic through latest Eocene (166–35 Ma). *Earth-Science Reviews*, **88**(3-4): 145–166.

Andersen NM. 1982. The Semiaquatic Bugs (Hemiptera, Gerromorpha): Phylogeny, Adaptations, Biogeography and Classification. Klampenborg: Scandinavian Science Press.

Andersen NM. 2000. A new species of Tetraripis from Thailand, with a critical assessment of the generic classification of the subfamily Rhagoveliinae (Hemiptera, Gerromorpha, Veliidae). *Tijdschrift Voor Entomologie*, **142**: 185–194.

Andersen NM, Weir TA. 2004. Mesoveliidae, Hebridae, and Hydrometridae of Australia (Hemiptera: Heteroptera: Gerromorpha), with a reanalysis of the phylogeny of semiaquatic bugs. *Invertebrate Systematics*, **18**(4): 467–522.

Beck RA, Burbank DW, Sercombe WJ, et al. 1995. Stratigraphic evidence for an early collision between northwest India and Asia. *Nature*, **373**(6509): 55–58.

Bossuyt F, Brown RM, Hillis DM, et al. 2006. Phylogeny and biogeography of a cosmopolitan frog radiation: late Cretaceous diversification resulted in continent-scale endemism in the family Ranidae. *Systematic Biology*, **55**(4): 579–594.

Bouckaert R, Heled J, Kühnert D, et al. 2014. BEAST 2: a software platform for Bayesian evolutionary analysis. *PLoS Computational Biology*, **10**(4): e1003537.

Camacho C, Coulouris G, Avagyan V, et al. 2009. BLAST+: architecture and applications. *BMC Bioinformatics*, **10**: 421.

Chatterjee S, Goswami A, Scotese CR. 2013. The longest voyage: tectonic, magmatic, and paleoclimatic evolution of the Indian plate during its northward flight from Gondwana to Asia. *Gondwana Research*, **23**(1): 238–267.

Damgaard J. 2008. Phylogeny of the semiaquatic bugs (Hemiptera-Heteroptera, Gerromorpha). *Insect Systematics & Evolution*, **39**(4): 431–460.

Damgaard J. 2012. What do we know about the phylogeny of the semi-aquatic bugs (Hemiptera: Heteroptera: Gerromorpha)?. *Entomologica Americana*, **118**(1): 81–98.

Datta-Roy A, Karanth KP. 2009. The out-of-India hypothesis: what do molecules suggest?. *Journal of Biosciences*, **34**(5): 687–697.

Drummond AJ, Ho SYW, Phillips MJ, et al. 2006. Relaxed phylogenetics and dating with confidence. *PLoS Biology*, **4**(5): e88.

Favre A, Päckert M, Pauls SU, et al. 2015. The role of the uplift of the Qinghai-Tibetan Plateau for the evolution of Tibetan biotas. *Biological Reviews*, **90**(1): 236–253.

Foley S, Krehenwinkel H, Cheng DQ, et al. 2021. Phylogenomic analyses reveal a Gondwanan origin and repeated out of India colonizations into Asia by tarantulas (Araneae: Theraphosidae). *PeerJ*, **9**: e11162.

Goloboff PA, Catalano SA. 2016. TNT version 1.5, including a full implementation of phylogenetic morphometrics. *Cladistics*, **32**(3): 221–238.

Gorin VA, Solovyeva EN, Hasan M, et al. 2020. A little frog leaps a long way: compounded colonizations of the Indian Subcontinent discovered in the tiny Oriental frog genus *Microhyla* (Amphibia: Microhylidae). *PeerJ*, **8**: e9411.

Gower DJ, Kupfer A, Oommen OV, et al. 2002. A molecular phylogeny of *Ichthyophiid caecilians* (Amphibia: Gymnophiona: Ichthyophiidae): out of India or out of South East Asia?. *Proceedings of the Royal Society B: Biological Sciences*, **269**(1500): 1563–1569.

Grismer JL, Schulte JA, Alexander A, et al. 2016. The Eurasian invasion: phylogenomic data reveal multiple Southeast Asian origins for Indian dragon lizards. *BMC Evolutionary Biology*, **16**: 43.

Hahn C, Bachmann L, Chevreux B. 2013. Reconstructing mitochondrial genomes directly from genomic next-generation sequencing reads-a baiting and iterative mapping approach. *Nucleic Acids Research*, **41**(13): e129.

Hall R. 2013. The palaeogeography of Sundaland and Wallacea since the Late Jurassic. *Journal of Limnology*, **72**(s2): 1–17.

He L, Wagner ND, Hörandl E. 2021. Restriction-site associated DNA sequencing data reveal a radiation of willow species (*Salix* L. , Salicaceae) in the Hengduan Mountains and adjacent areas. *Journal of Systematics and Evolution*, **59**(1): 44–57.

Ho SYW, Phillips MJ. 2009. Accounting for calibration uncertainty in phylogenetic estimation of evolutionary divergence times. *Systematic Biology*, **58**(3): 367–380.

Huxley TH. 1868. On the classification and distribution of the Alectoromorphae and Heteromorphae. *Proceedings of the Zoological Society of London*, 296–319.

Jiang YL, Yue L, Yang F, et al. 2022. Similar pattern, different paths: tracing the biogeographical history of Megaloptera (Insecta: Neuropterida) using mitochondrial phylogenomics. *Cladistics*, **38**(3): 374–391.

Kalyaanamoorthy S, Minh BQ, Wong TKF, et al. 2017. ModelFinder: fast model selection for accurate phylogenetic estimates. *Nature Methods*, **14**(6): 587–589.

Katoh K, Standley DM. 2013. MAFFT multiple sequence alignment software version 7: improvements in performance and usability. *Molecular Biology and Evolution*, **30**(4): 772–780.

Keast A. 1971. Continental drift and the evolution of the biota on southern continents. *The Quarterly Review of Biology*, **46**(4): 335–378.

Klaus S, Morley RJ, Plath M, et al. 2016. Biotic interchange between the Indian subcontinent and mainland Asia through time. *Nature Communications*, **7**: 12132.

Klaus S, Schubart CD, Streit B, et al. 2010. When Indian crabs were not yet Asian-biogeographic evidence for Eocene proximity of India and Southeast Asia. *BMC Evolutionary Biology*, **10**: 287.

Klaus S, Selvandran S, Goh JW, et al. 2013. Out of Borneo: neogene diversification of Sundaic freshwater crabs (Crustacea: Brachyura: Gecarcinucidae: *Parathelphusa*). *Journal of Biogeography*, **40**(1): 63–74.

Kou YX, Fan DM, Cheng SM, et al. 2023. Peripatric speciation within *Torreya fargesii* (Taxaceae) in the Hengduan Mountains inferred from multi-loci phylogeography. *BMC Ecology and Evolution*, **23**(1): 74.

Landis MJ, Matzke NJ, Moore BR, et al. 2013. Bayesian analysis of biogeography when the number of areas is large. *Systematic Biology*, **62**(6): 789–804.

Li FY, Shao LL, Li SQ. 2020. Tropical niche conservatism explains the Eocene migration from India to Southeast Asia in ochyroceratid spiders. *Systematic Biology*, **69**(5): 987–998.

Li JT, Li Y, Klaus S, et al. 2013. Diversification of rhacophorid frogs provides evidence for accelerated faunal exchange between India and Eurasia during the Oligocene. *Proceedings of the National Academy of Sciences of the United States of America*, **110**(9): 3441–3446.

Liu XY, Wang YJ, Shih C, et al. 2012. Early evolution and historical biogeography of fishflies (Megaloptera: Chauliodinae): implications from a phylogeny combining fossil and extant taxa. *PLoS One*, **7**(7): e40345.

Lohman DJ, de Bruyn M, Page T, et al. 2011. Biogeography of the indo-australian archipelago. *Annual Review of Ecology, Evolution, and Systematics*, **42**: 205–226.

Loria SF, Prendini L. 2020. Out of India, thrice: diversification of Asian forest scorpions reveals three colonizations of Southeast Asia. *Scientific Reports*, **10**(1): 22301.

Lundblad O. 1933. Zur Kenntnis der aquatilen und semiaquatilen Hemipteren von Sumatra, Java und Bali. *Archiv für Hydrobiologie*, **12 Supplement**: 1–195, 263–489.

Maliet O, Hartig F, Morlon H. 2019. A model with many small shifts for estimating species-specific diversification rates. *Nature Ecology & Evolution*, **3**(7): 1086–1092.

Matzke NJ. 2014. Model selection in historical biogeography reveals that

founder-event speciation is a crucial process in island clades. *Systematic Biology*, **63**(6): 951–970.
Meng GL, Li YY, Yang CT, et al. 2019. MitoZ: a toolkit for animal mitochondrial genome assembly, annotation and visualization. *Nucleic Acids Research*, **47**(11): e63.
Minh BQ, Schmidt HA, Chernomor O, et al. 2020. IQ-TREE 2: new models and efficient methods for phylogenetic inference in the genomic era. *Molecular Biology and Evolution*, **37**(5): 1530–1534.
Morley RJ. 2018. Assembly and division of the South and South-East Asian flora in relation to tectonics and climate change. *Journal of Tropical Ecology*, **34**(4): 209–234.
Nixon KC. 2002. WinClada, version1.00. 08. New York: Ithaca.
Palmieri L, Giribet G, Sharma PP. 2023. Too early for the ferry: the biogeographic history of the Assamiidae of southeast Asia (Chelicerata: Opiliones, Laniatores). *Molecular Phylogenetics and Evolution*, **178**: 107647.
Peng Y, Leung HCM, Yiu SM, et al. 2012. IDBA-UD: a *de novo* assembler for single-cell and metagenomic sequencing data with highly uneven depth. *Bioinformatics*, **28**(11): 1420–1428.
Polhemus DA. 1997. Systematics, phylogeny and zoogeography of the genus Rhagovelia (Heteroptera: Veliidae) in the Western Hemisphere (exclusive of the angustipes complex). *Thomas Say Publications in Entomology: Monographs, Entomological Society of America*, 386.
Rabosky DL, Grundler M, Anderson C, et al. 2014. BAMMtools: an R package for the analysis of evolutionary dynamics on phylogenetic trees. *Methods in Ecology and Evolution*, **5**(7): 701–707.
Rabosky DL, Santini F, Eastman J, et al. 2013. Rates of speciation and morphological evolution are correlated across the largest vertebrate radiation. *Nature Communications*, **4**: 1958.
Rambaut A, Drummond AJ, Xie D, et al. 2018. Posterior summarization in Bayesian phylogenetics using Tracer 1.7. *Systematic Biology*, **67**: 901–904.
Ree RH, Sanmartín I. 2018. Conceptual and statistical problems with the DEC+J model of founder-event speciation and its comparison with DEC via model selection. *Journal of Biogeography*, **45**(4): 741–749.
Ree RH, Smith SA. 2008. Maximum likelihood inference of geographic range evolution by dispersal, local extinction, and cladogenesis. *Systematic Biology*, **57**(1): 4–14.
Ronquist F. 1997. Dispersal-vicariance analysis: a new approach to the quantification of historical biogeography. *Systematic Biology*, **46**(1): 195–203.
Sholihah A, Delrieu-Trottin E, Condamine FL, et al. 2021a. Impact of Pleistocene eustatic fluctuations on evolutionary dynamics in Southeast Asian biodiversity hotspots. *Systematic Biology*, **70**(5): 940–960.
Sholihah A, Delrieu-Trottin E, Sukmono T, et al. 2021b. Limited dispersal and in situ diversification drive the evolutionary history of Rasborinae fishes in Sundaland. *Journal of Biogeography*, **48**(9): 2153–2173.
Sitam FT, Salgado-Lynn M, Denel A, et al. 2023. Phylogeography of the Sunda pangolin, *Manis javanica*: implications for taxonomy, conservation management and wildlife forensics. *Ecology and Evolution*, **13**(8): e10373.
Talavera G, Castresana J. 2007. Improvement of phylogenies after removing divergent and ambiguously aligned blocks from protein sequence alignments. *Systematic Biology*, **56**(4): 564–577.
Torsvik TH, Cocks LRM. 2013. Gondwana from top to base in space and time. *Gondwana Research*, **24**(3-4): 999–1030.
van Hinsbergen DJJ, Lippert PC, Dupont-Nivet G, et al. 2012. Greater India Basin hypothesis and a two-stage Cenozoic collision between India and Asia. *Proceedings of the National Academy of Sciences of the United States of America*, **109**(20): 7659–7664.
Wu XY, Hu JS, Chen L, et al. 2023. Paleogene India-Eurasia collision constrained by observed plate rotation. *Nature Communications*, **14**(1): 7272.
Xing YW, Ree RH. 2017. Uplift-driven diversification in the Hengduan Mountains, a temperate biodiversity hotspot. *Proceedings of the National Academy of Sciences of the United States of America*, **114**(17): E3444–E3451.
Xu X, Su YC, Ho SYW, et al. 2021. Phylogenomic analysis of ultraconserved elements resolves the evolutionary and biogeographic history of segmented trapdoor spiders. *Systematic Biology*, **70**(6): 1110–1122.
Yamahira K, Ansai S, Kakioka R, et al. 2021. Mesozoic origin and 'out-of-India' radiation of ricefishes (Adrianichthyidae). *Biology Letters*, **17**(8): 20210212.
Ye Z, Chen PP, Bu WJ. 2013. Contribution to the knowledge on the Oriental genus *Perittopus* Fieber, 1861 (Hemiptera: Heteroptera: Veliidae) with descriptions of four new species from China and Thailand. *Zootaxa*, **3616**(1): 31–48.
Ye Z, Jin ZZ, Polhemus DA, et al. 2024. Phylogenomic reconstruction illuminates the evolutionary history of freshwater to marine transition in the subfamily Haloveliinae (Hemiptera: Heteroptera: Veliidae). *Systematic Entomology*, **49**(2): 330–343.
Ye Z, Qiao M, Jin ZZ, et al. 2020. Notes on the genus *Perittopus* Fieber, 1860 (Hemiptera: Heteroptera: Veliidae) with descriptions of three new species from Indochina. *Zootaxa*, **4858**(3): 417–426.
Yin A, Harrison TM. 2000. Geologic evolution of the Himalayan-Tibetan orogen. *Annual Review of Earth and Planetary Sciences*, **28**: 211–280.
Yuan ZY, Zhang BL, Raxworthy CJ, et al. 2019. Natatanuran frogs used the Indian Plate to step-stone disperse and radiate across the Indian Ocean. *National Science Review*, **6**(1): 10–14.
Zenz K, Zettel H. 2021. A redescription of *Perittopus maculatus* Paiva, 1919 (Insecta: Hemiptera: Veliidae) from India. *Annalen des Naturhistorischen Museums in Wien, Serie B*, **123**: 257–262.
Zettel H. 2001a. Five new species of *Perittopus* Fieber, 1861 (Hemiptera: Veliidae) from Southeast Asia. *The Raffles Bulletin of Zoology*, **49**(1): 109–119.
Zettel H. 2001b. *Perittopus ceylanicus* sp. n. , first record of the subfamily Perittopinae (Insecta: Heteroptera: Veliidae) from Sri Lanka. *Annalen des Naturhistorischen Museums in Wien, Serie B*, **103**: 269–271.
Zettel H. 2011. A contribution to the knowledge of Gerromorpha (Insecta: Hemiptera) of Myanmar, with seven new species, eight new records, and a catalogue. *Annalen des Naturhistorischen Museums in Wien, Serie B*, **112**: 89–114.
Zhang D, Gao FL, Jakovlić I, et al. 2020. PhyloSuite: an integrated and scalable desktop platform for streamlined molecular sequence data management and evolutionary phylogenetics studies. *Molecular Ecology Resources*, **20**(1): 348–355.
Zhang H, Zhong Y, Zhu Y, et al. 2024. The evolutionary history of *Sinopoda* spiders (Sparassidae: Heteropodinae): out of the Himalayas and down the mountain slopes. *Ecography*, **2024**(11): e06873.
Zhao YJ, Yin GS, Pan YZ, et al. 2021. Climatic Refugia and Geographical Isolation Contribute to the Speciation and Genetic Divergence in Himalayan-Hengduan Tree Peonies (*Paeonia delavayi* and *Paeonia ludlowii*). *Frontiers in Genetics*, **11**: 595334.